

# Scattering of finite-size anisotropic metastructures via the relaxed micromorphic model

Alexios Aivaliotis<sup>1</sup>, Domenico Tallarico<sup>2</sup>, Ali Daouadji<sup>3</sup>, Patrizio Neff<sup>4</sup>  
and Angela Madeo<sup>5</sup>

June 18, 2022

## Abstract

The conception of new metamaterials showing unorthodox behaviors with respect to elastic wave propagation has become possible in recent years thanks to powerful dynamical homogenization techniques. Such methods effectively allow to describe the behavior of an infinite medium generated by periodically architected base materials. Nevertheless, when it comes to the study of the scattering properties of finite-sized structures, dealing with the correct boundary conditions at the macroscopic scale becomes challenging. In this paper, we show how finite-domain boundary value problems can be set-up in the framework of enriched continuum mechanics (relaxed micromorphic model) by imposing continuity of macroscopic displacement and of generalized traction when non-local effects are neglected.

The case of a metamaterial slab of finite width is presented, its scattering properties are studied via a semi-analytical solution of the relaxed micromorphic model and compared to numerical simulations encoding all details of the selected microstructure. The reflection coefficient obtained via the two methods is presented as a function of the frequency and of the direction of propagation of the incident wave. We find excellent agreement for a large range of frequencies going from the long-wave limit to frequencies beyond the first band-gap and for angles of incidence ranging from normal to near parallel incidence. The case of a semi-infinite metamaterial is also presented and is seen to be a reliable measure of the average behavior of the finite metastructure. A tremendous gain in terms of computational time is obtained when using the relaxed micromorphic model for the study of the considered metastructure.

**Keywords:** enriched continuum mechanics, anisotropic metamaterials, band-gaps, wave-propagation, relaxed micromorphic model, interface, scattering, finite-sized metastructures.

**AMS 2010 subject classification:** 74A30 (nonsimple materials), 74A60 (micromechanical theories), 74B05 (classical linear elasticity), 74J05 (linear waves), 74J10 (bulk waves), 75J15 (surface waves), 74J20 (wave scattering), 74M25 (micromechanics), 74Q15 (effective constitutive equations).

---

<sup>1</sup>Alexios Aivaliotis, corresponding author, alexios.aivaliotis@insa-lyon.fr, GEOMAS, INSA-Lyon, Université de Lyon, 20 avenue Albert Einstein, 69621, Villeurbanne cedex, France

<sup>2</sup>Domenico Tallarico, domenico.tallarico@gmail.com, GEOMAS, INSA-Lyon, Université de Lyon, 20 avenue Albert Einstein, 69621, Villeurbanne Cedex, France

<sup>3</sup>Ali Daouadji, ali.daouadji@insa-lyon.fr, GEOMAS, INSA-Lyon, Université de Lyon, 20 avenue Albert Einstein, 69621, Villeurbanne Cedex, France

<sup>4</sup>Patrizio Neff, patrizio.neff@uni-due.de, Head of Chair for Nonlinear Analysis and Modelling, Fakultät für Mathematik, Universität Duisburg-Essen, Mathematik-Carrée, Thea-Leymann-Straße 9, 45127 Essen, Germany

<sup>5</sup>Angela Madeo, angela.madeo@insa-lyon.fr, GEOMAS, INSA-Lyon, Université de Lyon, 20 avenue Albert Einstein, 69621, Villeurbanne Cedex, France

# Contents

<b>1</b>	<b>Introduction</b>	<b>2</b>
1.1	Notation . . . . .	4
<b>2</b>	<b>Governing equations and Energy flux</b>	<b>5</b>
2.1	The classical isotropic Cauchy continuum . . . . .	5
2.2	The anisotropic relaxed micromorphic model . . . . .	5
2.3	The plane-strain tetragonal symmetry case . . . . .	6
<b>3</b>	<b>Bulk wave propagation in Cauchy and relaxed micromorphic continua</b>	<b>7</b>
3.1	Isotropic Cauchy continuum . . . . .	7
3.2	Relaxed micromorphic continuum . . . . .	8
<b>4</b>	<b>Boundary Conditions</b>	<b>9</b>
4.1	Boundary conditions at an interface between a Cauchy continuum and a relaxed micromorphic continuum with vanishing characteristic length $L_c = 0$ . . . . .	9
4.1.1	Continuity of macroscopic displacement and of generalized force implies conservation of energy at the interface . . . . .	10
4.2	Boundary conditions for a micromorphic slab embedded between two Cauchy media . . . . .	11
<b>5</b>	<b>Reflection and transmission at the single interface</b>	<b>11</b>
<b>6</b>	<b>Reflection and transmission at a relaxed micromorphic slab</b>	<b>12</b>
<b>7</b>	<b>Reflective properties of a micro-structured slab</b>	<b>13</b>
7.1	Bloch-Floquet conditions . . . . .	15
7.2	Reflectance . . . . .	15
<b>8</b>	<b>Results and discussion</b>	<b>16</b>
8.1	Scattering at a relaxed micromorphic slab . . . . .	17
8.2	Scattering at a single relaxed micromorphic interface: Some hints towards negative-refraction-like phenomena in enriched continua . . . . .	20
<b>9</b>	<b>Conclusions</b>	<b>23</b>
<b>A</b>	<b>Appendix</b>	<b>24</b>
A.1	Energy flux for the anisotropic relaxed micromorphic model . . . . .	24
A.1.1	Derivation of expression (2.10) . . . . .	24
A.1.2	Analytical expression of the flux for the relaxed micromorphic model when $L_c = 0$ . . . . .	25
A.2	The matrix $\hat{A}$ . . . . .	25
A.3	Lemma 1 . . . . .	26

## 1 Introduction

Recent years have seen the rapid development of mechanical metamaterials and phononic crystals showing unorthodox behaviors with respect to elastic wave propagation, including focusing, channeling, cloaking, filtering, etc. [8, 9, 14, 27, 31]. The basic idea underlying the design of these metamaterials is that of suitably engineering the architecture of their microstructure in such a way that the resulting macroscopic (homogenized) properties can exhibit the desired exotic characteristics. One of the most impressive features provided by such metamaterials is that of showing band-gaps, i.e. frequency ranges for which wave propagation is inhibited. The most widespread class of metamaterials consists of those which are obtained by a periodic repetition in space of a specific unit cell and which are known as periodic metamaterials. For such metamaterials, renown scientists have provided analytical [37, 38, 39, 40] or numerical [13] homogenization techniques (in the spirit of the seminal works of Bloch [7] and Floquet [12]), allowing to obtain a homogenized model which suitably describes, to a good extent, the dynamical behavior of the bulk periodic metamaterial at the macroscopic scale. Rigorous models for studying the macroscopic mechanical behavior of non-periodic structures become rarer and usually rely on the use

of detailed finite element modeling of the considered microstructures (see e.g. [15]), thus rendering the implementation of large structures computationally demanding and impractical.

At the current state of knowledge, little effort is made in trying to model large metamaterial structures (which we will call *metastructures*), due to the difficulty of imposing suitably boundary conditions in the framework of homogenization theories (see [36]). We propose to shed new light in this direction by the introduction of an enriched continuum model of the micromorphic type (relaxed micromorphic model), equipped with the proper boundary conditions for the effective description of finite sized band-gap metastructures. The relaxed micromorphic model (see [2, 4, 5, 10, 17, 18, 19, 20, 21, 22, 23, 24, 25, 28, 29, 30] for preliminary results) has a simplified structure which allows to describe the homogenized properties of (periodic or even non-periodic) anisotropic metamaterials with a limited number of constant material parameters and for an extended frequency range going from the long-wave limit to frequencies which are beyond the first band-gap. The rigorous development of the relaxed micromorphic model for anisotropic metamaterials has been given in [10], where applications to different classes of symmetry and the particular case of tetragonal periodic metamaterials are also discussed. In the latter paper, a procedure to univocally determine some of the material parameters for periodic metamaterials with static tests is also provided. It is important to point out that the relaxed micromorphic model is not obtained via a formal homogenization procedure, but is developed generalizing the framework of macroscopic continuum elasticity by introducing enriched kinematics and enhanced constitutive laws for the strain energy density. In this way, extra degrees of freedom are added to the classical macroscopic displacement via the introduction of the micro-distortion tensor and the chosen constitutive form for the anisotropic strain energy density. This allows to introduce a limited number of elastic parameters through fourth-order macro and micro elasticity tensors working on the sym/skew orthogonal decomposition of the introduced deformation measures (see [10] for details). The need of using an enriched continuum model of the micromorphic type for describing the broadband macroscopic behavior of acoustic metamaterials as emerging from a numerical homogenization technique was recently proven in [35]. Nevertheless, the authors of the latter paper showed that a huge number of elastic parameters (up to 600 for the studied tetragonal two-dimensional structures) is indeed needed to perform an accurate fitting of the dispersion curves issued by the Bloch-Floquet analysis. This extensive number of parameters can also be found in other micromorphic models of the Eringen [11] and Mindlin [26] type. The need of this vast number of parameters is related to the fact that the macroscopic class of symmetry of the metamaterial and the correct (i.e. sym/skew-decomposed) deformation measures are usually not accounted for. As a matter of fact, the relaxed micromorphic model, as proposed in [10], is able to minimize the number of parameters (15 for the tetragonal 2D-case) thanks to the introduction of “generalized classes of symmetry” for metamaterials and to the sym/skew-decomposition choice of the introduced deformation measures. The fitting of the dispersion curves, which can be obtained by the inverse fitting procedure proposed in [10], cannot reproduce point-by-point the dispersion curves issued via Bloch-Floquet analysis (which is not the aim of our work), but is general enough to capture the main features of the studied metamaterials’ behavior including dispersion, anisotropy, band-gaps for a wide range of frequencies and for wavelengths which can become very small and even comparable to the size of the unit cell.

Last, but most importantly, since it is issued by a variational procedure, the relaxed micromorphic model is naturally equipped with the correct macroscopic boundary conditions which have to be applied on the boundaries of the considered metamaterials. This implies that the global refractive properties of metamaterials’ boundaries can be described in the simplified framework of enriched continuum mechanics, thus providing important information while keeping simple enough to allow important computational time-saving.

Very complex phenomena take place when an incident elastic wave hits a metamaterial’s boundary, resulting in reflected and transmitted waves which can be propagative or evanescent depending on the frequency and angle of incidence of the incident wave itself. The primordial importance of evanescent (non-propagative) waves for the correct formulation of boundary value problems for metamaterials has been highlighted in [36, 41], where the need of infinite evanescent modes for obtaining continuity of displacement and of tractions at the considered metamaterial’s boundary is pointed out. One of the advantages of the enriched continuum model proposed in the present paper is that the generalized boundary conditions (continuity of macroscopic displacement and of generalized traction) associated to the considered boundary value problem are exactly fulfilled with a finite number of modes.

We will show that the proposed framework allows to describe, to a good extent, the overall behavior of the reflection coefficient (generated by a plane incident wave) of an interface between a homogeneous medium and a specific tetragonal band-gap metamaterial (both considered as semi-infinite in space), as function of the frequency and of the angle of incidence of the incident wave. Moreover, given the

auto-consistency of bulk PDEs and associated jump conditions, we are able to treat the more realistic case of a metamaterial slab of finite width treated as an inclusion between two semi-infinite homogeneous media. Also for the latter case, we are able to obtain the reflective properties of the slab as a function of the frequency and angle of incidence of the plane incident wave. To the authors' knowledge, a boundary value problem which describes the dynamical behavior of realistic finite-size metamaterial structures via the introduction of rigorous macroscopic boundary conditions, is presented here for the first time.

The results show very good agreement (for a wide range of frequencies extending from the low-frequency Cauchy limit to frequencies beyond the first band-gap and for all the possible angles of incidence) with the direct FEM numerical implementation of the considered system in COMSOL, where the detailed geometry of the unit cell has been implemented in the framework of classical linear elasticity. We observe a tremendous advantage in terms of the computational time needed to perform the numerical simulations (few hours for the relaxed micromorphic model against weeks for the direct FEM simulation).

We structure the paper as follows: In Section 1 we present an introduction together with the notation used throughout the paper. Section 2 briefly recalls the governing equations describing the motion of Cauchy and relaxed micromorphic continua, with specific reference to the definition of the energy flux for both cases. In Section 3 the plane-wave solutions for the Cauchy and relaxed micromorphic continua are obtained as solutions of the corresponding eigenvalue problems. In Section 4 we provide essential information concerning the correct boundary conditions which have to be imposed at the metamaterial's boundaries, in the relaxed micromorphic framework. In Sections 5 and 6 the problems of the scattering from a relaxed micromorphic single interface and relaxed micromorphic slab of finite size, respectively, are rigorously set up and solved. Section 7 presents the detailed implementation of the microstructured metamaterial slab based on classical elasticity and implemented in the commercial Finite Element software COMSOL Multiphysics. Section 8 thoroughly presents our results by means of a detailed discussion. Section 9 is devoted to conclusions and perspectives.

## 1.1 Notation

Let  $\mathbb{R}^{3 \times 3}$  be the set of all real  $3 \times 3$  second order tensors which we denote by capital letters. A simple and a double contraction between tensors of any suitable order is denoted by  $\cdot$  and  $:$  respectively, while the scalar product of tensors of suitable order is denoted by  $\langle \cdot, \cdot \rangle$ .<sup>1</sup> The Einstein sum convention is implied throughout this text unless otherwise specified. The standard Euclidean scalar product on  $\mathbb{R}^{3 \times 3}$  is given by  $\langle X, Y \rangle = \text{tr}(X \cdot Y^T)$  and consequently the Frobenius tensor norm is  $\|X\|^2 = \langle X, X \rangle$ . The identity tensor on  $\mathbb{R}^{3 \times 3}$  will be denoted by  $\mathbb{1}$ ; then,  $\text{tr}(X) = \langle X, \mathbb{1} \rangle$ .

We denote by  $B_L$  a bounded domain in  $\mathbb{R}^3$ , by  $\partial B_L$  its regular boundary and by  $\Sigma$  any material surface embedded in  $B_L$ . The outward unit normal to  $\partial B_L$  will be denoted by  $\nu$  as will the outward unit normal to a surface  $\Sigma$  embedded in  $B_L$ . Given a field  $a$  defined on the surface  $\Sigma$ , we define the jump of  $a$  through the surface  $\Sigma$  as:

$$[[a]] = a^+ - a^-, \quad \text{with} \quad a^- := \lim_{\substack{x \in B_L^- \setminus \Sigma \\ x \rightarrow \Sigma}} a, \quad \text{and} \quad a^+ := \lim_{\substack{x \in B_L^+ \setminus \Sigma \\ x \rightarrow \Sigma}} a, \quad (1.1)$$

where  $B_L^-, B_L^+$  are the two subdomains which result from splitting  $B_L$  by the surface  $\Sigma$ .

Classical gradient  $\nabla$  and divergence  $\text{Div}$  operators are used throughout the paper.<sup>2</sup> Moreover, we introduce the Curl operator of the matrix  $P$  as  $(\text{Curl } P)_{ij} = \epsilon_{jmn} P_{in,m}$ , where  $\epsilon_{jmn}$  denotes the standard Levi-Civita tensor, which is equal to  $+1$ , if  $(j, m, n)$  is an even permutation of  $(1, 2, 3)$ , to  $-1$ , if  $(j, m, n)$  is an odd permutation of  $(1, 2, 3)$ , or to  $0$  if  $j = m$ , or  $m = n$ , or  $n = j$ .

Given a time interval  $[0, T]$ , the classical macroscopic displacement field is denoted by:

$$u(x, t) = (u_1(x, t), u_2(x, t), u_3(x, t))^T, \quad x \in B_L, \quad t \in [0, T]. \quad (1.2)$$

In the framework of enriched continuum models of the micromorphic type, extra degrees of freedom are

<sup>1</sup>For example,  $(A \cdot v)_i = A_{ij} v_j$ ,  $(A \cdot B)_{ik} = A_{ij} B_{jk}$ ,  $A : B = A_{ij} B_{ji}$ ,  $(C \cdot B)_{ijk} = C_{ijp} B_{pk}$ ,  $(C : B)_i = C_{ijp} B_{pj}$ ,  $\langle v, w \rangle = v \cdot w = v_i w_i$ ,  $\langle A, B \rangle = A_{ij} B_{ij}$ , etc.

<sup>2</sup>The operators  $\nabla$ , curl and Div are the classical gradient, curl and divergence operators. In symbols, for a field  $u$  of any order,  $(\nabla u)_i = u_{,i}$ , for a vector field  $v$ ,  $(\text{curl } v)_i = \epsilon_{ijk} v_{k,j}$  and for a field  $w$  of order  $k > 1$ ,  $(\text{Div } w)_{i_1 i_2 \dots i_{k-1}} = w_{i_1 i_2 \dots i_k, i_k}$

added through the introduction of the micro-distortion tensor  $P$  denoted by:

$$P(x, t) = \begin{pmatrix} P_{11}(x, t) & P_{12}(x, t) & P_{13}(x, t) \\ P_{21}(x, t) & P_{22}(x, t) & P_{23}(x, t) \\ P_{31}(x, t) & P_{32}(x, t) & P_{33}(x, t) \end{pmatrix}, \quad x \in B_L, \quad t \in [0, T]. \quad (1.3)$$

## 2 Governing equations and Energy flux

### 2.1 The classical isotropic Cauchy continuum

The equations of motions in strong form for a classical Cauchy continuum are:

$$\rho u_{,tt} = \text{Div } \sigma, \quad \rho u_{i,tt} = \sigma_{ij,j}, \quad (2.1)$$

where

$$\sigma = 2\mu \text{sym } \nabla u + \lambda \text{tr}(\text{sym } \nabla u) \mathbb{1}, \quad \sigma_{ij} = \mu(u_{i,j} + u_{j,i}) + \lambda u_{k,k} \delta_{ij}, \quad (2.2)$$

is the classical symmetric Cauchy stress tensor for isotropic materials and  $\mu$  and  $\lambda$  are the classical Lamé parameters.

The mechanical system we are considering is conservative and, therefore, the energy must be conserved in the sense that the following differential form of a continuity equation must hold:

$$E_{,t} + \text{div} H = 0, \quad (2.3)$$

where  $E$  is the total energy of the system and  $H$  is the energy flux vector, whose explicit expression is given by (see e.g. [2] for a detailed derivation)

$$H = -\sigma \cdot u_{,t}, \quad H_k = -\sigma_{ik} u_{k,t}. \quad (2.4)$$

### 2.2 The anisotropic relaxed micromorphic model

The kinetic energy density in the anisotropic relaxed micromorphic model considered in this paper is [10]:

$$\begin{aligned} J(u_{,t}, \nabla u_{,t}, P_{,t}) &= \frac{1}{2} \rho \langle u_{,t}, u_{,t} \rangle + \frac{1}{2} \langle \mathbb{J}_{\text{micro}} \text{sym } P_{,t}, \text{sym } P_{,t} \rangle + \frac{1}{2} \langle \mathbb{J}_c \text{skew } P_{,t}, \text{skew } P_{,t} \rangle \\ &+ \frac{1}{2} \langle \mathbb{T}_e \text{sym } \nabla u_{,t}, \text{sym } \nabla u_{,t} \rangle + \frac{1}{2} \langle \mathbb{T}_c \text{skew } \nabla u_{,t}, \text{skew } \nabla u_{,t} \rangle, \end{aligned} \quad (2.5)$$

where  $u$  is the macroscopic displacement field,  $P \in \mathbb{R}^{3 \times 3}$  is the non-symmetric micro-distortion tensor and  $\rho$  is the apparent macroscopic density. Moreover,  $\mathbb{J}_e, \mathbb{J}_{\text{micro}}, \mathbb{J}_c, \mathbb{T}_e$  and  $\mathbb{T}_c$  are 4th order inertia tensors, whose precise form will be specified in the following. An existence and uniqueness result for models with these types of generalized inertia terms is given in [32].

The strain energy density for an anisotropic relaxed micromorphic medium is given by [10]:

$$\begin{aligned} W(\nabla u, P, \text{Curl } P) &= \frac{1}{2} \langle \mathbb{C}_e \text{sym}(\nabla u - P), \text{sym}(\nabla u - P) \rangle + \frac{1}{2} \langle \mathbb{C}_{\text{micro}} \text{sym } P, \text{sym } P \rangle \\ &+ \frac{1}{2} \langle \mathbb{C}_c \text{skew}(\nabla u - P), \text{skew}(\nabla u - P) \rangle \\ &+ \frac{L_c^2}{2} (\langle \mathbb{L}_e \text{sym } \text{Curl } P, \text{sym } \text{Curl } P \rangle + \langle \mathbb{L}_c \text{skew } \text{Curl } P, \text{skew } \text{Curl } P \rangle), \end{aligned} \quad (2.6)$$

where  $\mathbb{C}_e, \mathbb{C}_{\text{micro}}, \mathbb{C}_c, \mathbb{L}_e$  and  $\mathbb{L}_c$  are 4th order elasticity tensors which will be precisely defined in the following. Moreover,  $L_c$  is a characteristic length, which may account for non-local effects in the metamaterial. We remark that non-local effects provide small corrections to the average behavior of the metamaterial, so that only a small error is introduced if in a first instance, non-localities are neglected.

Let  $t_0 > 0$  be a fixed time and consider a bounded domain  $B_L \subset \mathbb{R}^3$ . The minimization of the action functional of the system at hand is defined as

$$\mathcal{A} = \int_0^{t_0} \int_{B_L} (J - W) dX dt, \quad (2.7)$$

where  $J$  is the kinetic and  $W$  the strain energy of the system, defined by (2.5) and (2.6), respectively. The action functional ([10]) provides the governing equations for the anisotropic relaxed micromorphic model:

$$\begin{aligned} \rho u_{,tt} - \text{Div } \hat{\sigma}_{,tt} &= \text{Div } \tilde{\sigma}, \\ \mathbb{J}_{\text{micro}} \text{sym } P_{,tt} &= \tilde{\sigma}_e - s - \text{sym Curl } m, \quad \mathbb{J}_c \text{skew } P_{,tt} = \tilde{\sigma}_c - \text{skew Curl } m, \end{aligned} \quad (2.8)$$

where we set

$$\begin{aligned} \tilde{\sigma}_e &= \mathbb{C}_e \text{sym}(\nabla u - P), \quad \tilde{\sigma}_c = \mathbb{C}_c \text{skew}(\nabla u - P), \quad \tilde{\sigma} = \tilde{\sigma}_e + \tilde{\sigma}_c, \quad \hat{\sigma} = \mathbb{T}_e \text{sym } \nabla u + \mathbb{T}_c \text{skew } \nabla u, \\ s &= \mathbb{C}_{\text{micro}} \text{sym } P, \quad m := L_c^2 (\mathbb{L}_e \text{sym Curl } P + \mathbb{L}_c \text{skew Curl } P). \end{aligned} \quad (2.9)$$

Conservation of energy for an anisotropic relaxed micromorphic continuum is formally written as in equation (2.3). The specific form for the energy flux for an anisotropic relaxed micromorphic continuum is (see Appendix A.1.1 for detailed derivation of this expression)

$$H = -(\tilde{\sigma} + \hat{\sigma})^T \cdot u_{,t} - (m^T \cdot P_t) : \epsilon, \quad H_k = -u_{i,t} (\tilde{\sigma}_{ik} + \hat{\sigma}_{ik}) - m_{ih} P_{ij,t} \epsilon_{jhk}. \quad (2.10)$$

From here on, we set  $L_c = 0$  for the remainder of this article. Indeed, it will be shown that even if non-locality is switched off ( $L_c = 0$ ), the relaxed micromorphic model is able to capture the more relevant features of the considered problem. Taking the internal length into account provides small corrections to the overall behavior of the metamaterial. Such effects will be discussed in forthcoming papers.

### 2.3 The plane-strain tetragonal symmetry case

In this article, we are interested in plane-strain solutions of the system (2.8). This means that the macroscopic displacement  $u$  and the micro-distortion tensor  $P$  introduced in (1.2) and (1.3) are supposed to take the following form:

$$u = u(x_1, x_2) = (u_1(x_1, x_2), u_2(x_1, x_2), 0)^T, \quad \text{and} \quad u_{i,3} = 0, \quad i = 1, 2, \quad (2.11)$$

and

$$P = P(x_1, x_2) = \begin{pmatrix} P_{11}(x_1, x_2) & P_{12}(x_1, x_2) & 0 \\ P_{21}(x_1, x_2) & P_{22}(x_1, x_2) & 0 \\ 0 & 0 & 0 \end{pmatrix}, \quad \text{and} \quad P_{ij,3} = 0, \quad i = 1, 2, \quad j = 1, 2. \quad (2.12)$$

Following [10], we denote the second order constitutive tensors in Voigt notation corresponding to the fourth order ones appearing in the kinetic and strain energy expressions (2.5) and (2.6) by a tilde.<sup>3</sup> For the tetragonal case, the constitutive tensors in Voigt notation are (see [4, 10])

$$\begin{aligned} \tilde{\mathbb{C}}_e &= \begin{pmatrix} 2\mu_e + \lambda_e & \lambda_e & \star & 0 & 0 & 0 \\ \lambda_e & 2\mu_e + \lambda_e & \star & 0 & 0 & 0 \\ \star & \star & \star & 0 & 0 & 0 \\ 0 & 0 & 0 & \star & 0 & 0 \\ 0 & 0 & 0 & 0 & \star & 0 \\ 0 & 0 & 0 & 0 & 0 & \mu_e^* \end{pmatrix}, \quad \tilde{\mathbb{C}}_{\text{micro}} = \begin{pmatrix} 2\mu_{\text{micro}} + \lambda_{\text{micro}} & \lambda_{\text{micro}} & \star & 0 & 0 & 0 \\ \lambda_{\text{micro}} & 2\mu_{\text{micro}} + \lambda_{\text{micro}} & \star & 0 & 0 & 0 \\ \star & \star & \star & 0 & 0 & 0 \\ 0 & 0 & 0 & \star & 0 & 0 \\ 0 & 0 & 0 & 0 & \star & 0 \\ 0 & 0 & 0 & 0 & 0 & \mu_{\text{micro}}^* \end{pmatrix}, \\ \tilde{\mathbb{C}}_c &= \begin{pmatrix} \star & 0 & 0 \\ 0 & \star & 0 \\ 0 & 0 & 4\mu_c \end{pmatrix}, \quad \tilde{\mathbb{J}}_{\text{micro}} = \begin{pmatrix} 2\eta_1 + \eta_3 & \eta_3 & \star & 0 & 0 & 0 \\ \eta_3 & 2\eta_1 + \eta_3 & \star & 0 & 0 & 0 \\ \star & \star & \star & 0 & 0 & 0 \\ 0 & 0 & 0 & \star & 0 & 0 \\ 0 & 0 & 0 & 0 & \star & 0 \\ 0 & 0 & 0 & 0 & 0 & \eta_1^* \end{pmatrix}, \quad \tilde{\mathbb{J}}_c = \begin{pmatrix} \star & 0 & 0 \\ 0 & \star & 0 \\ 0 & 0 & 4\eta_2 \end{pmatrix}, \end{aligned}$$

<sup>3</sup>For example, the 4th order tensor  $\mathbb{C}_e$  is written as  $\tilde{\mathbb{C}}_e$  in Voigt notation.

$$\tilde{\mathbb{T}}_e = \begin{pmatrix} 2\bar{\eta}_1 + \bar{\eta}_3 & \bar{\eta}_3 & \star & 0 & 0 & 0 \\ \bar{\eta}_3 & 2\bar{\eta}_1 + \bar{\eta}_3 & \star & 0 & 0 & 0 \\ \star & \star & \star & 0 & 0 & 0 \\ 0 & 0 & 0 & \star & 0 & 0 \\ 0 & 0 & 0 & 0 & \star & 0 \\ 0 & 0 & 0 & 0 & 0 & \bar{\eta}_1^* \end{pmatrix}, \quad \tilde{\mathbb{T}}_c = \begin{pmatrix} \star & 0 & 0 \\ 0 & \star & 0 \\ 0 & 0 & 4\bar{\eta}_2 \end{pmatrix},$$

where we denoted by a star those components, which work on out-of-plane macro- and micro-strains and do not play any role in the considered in plane (plane-strain) problem.

### 3 Bulk wave propagation in Cauchy and relaxed micromorphic continua

#### 3.1 Isotropic Cauchy continuum

We make the plane-wave ansatz for the solution to (2.1):

$$u(x_1, x_2, t) = \hat{\psi} e^{i(\langle k, x \rangle - \omega t)} = \hat{\psi} e^{i(k_1 x_1 + k_2 x_2 - \omega t)}, \quad \hat{\psi} \in \mathbb{C}^2, \quad (3.1)$$

where  $k = (k_1, k_2)^T$  is the wave vector and  $\omega$  is the angular frequency.<sup>4</sup> Plugging (3.1) into equation (2.1) we get a  $2 \times 2$  algebraic system of the form

$$A \cdot \hat{\psi} = 0, \quad (3.2)$$

where

$$A = \begin{pmatrix} \rho \omega^2 - (2\mu + \lambda) k_1^2 - \mu k_2^2 & -(\mu + \lambda) k_1 k_2 \\ -(\mu + \lambda) k_1 k_2 & \rho \omega^2 - (2\mu + \lambda) k_2^2 - \mu k_1^2 \end{pmatrix}. \quad (3.3)$$

The algebraic system (3.2) has a solution if and only if  $\det A = 0$ . This is a bi-quadratic polynomial equation which has the following four solutions:

$$k_1^{L,r} = -\sqrt{\frac{\rho}{2\mu + \lambda} \omega^2 - k_2^2}, \quad k_1^{S,r} = -\sqrt{\frac{\rho}{\mu} \omega^2 - k_2^2}, \quad k_1^{L,t} = \sqrt{\frac{\rho}{2\mu + \lambda} \omega^2 - k_2^2}, \quad k_1^{S,t} = \sqrt{\frac{\rho}{\mu} \omega^2 - k_2^2}, \quad (3.4)$$

where we denote by L and S the longitudinal and shear waves and by r and t whether they are “reflected” or “transmitted”, respectively. In a semi-infinite medium, the sign of these solutions must be chosen according to the direction of propagation of the considered wave. We plug the solutions (3.4) into (3.2) to calculate the corresponding eigenvectors

$$\hat{\psi}^{L,r} = \begin{pmatrix} 1 \\ -\frac{k_2^{L,r}}{k_1^{L,r}} \end{pmatrix}, \quad \hat{\psi}^{S,r} = \begin{pmatrix} 1 \\ \frac{k_1^{S,r}}{k_2^{S,r}} \end{pmatrix}, \quad \hat{\psi}^{L,t} = \begin{pmatrix} 1 \\ \frac{k_2^{L,t}}{k_1^{L,t}} \end{pmatrix}, \quad \hat{\psi}^{S,t} = \begin{pmatrix} 1 \\ -\frac{k_1^{S,t}}{k_2^{S,t}} \end{pmatrix}. \quad (3.5)$$

Normalizing these eigenvectors gives:

$$\psi^{L,r} := \frac{1}{|\hat{\psi}^{L,r}|} \hat{\psi}^{L,r}, \quad \psi^{S,r} := \frac{1}{|\hat{\psi}^{S,r}|} \hat{\psi}^{S,r}, \quad \psi^{L,t} := \frac{1}{|\hat{\psi}^{L,t}|} \hat{\psi}^{L,t}, \quad \psi^{S,t} := \frac{1}{|\hat{\psi}^{S,t}|} \hat{\psi}^{S,t}. \quad (3.6)$$

Then, the general solution to (2.1) can be written as:

$$u(x_1, x_2, t) = a^{L,r} \psi^{L,r} e^{i(k_1^{L,r} x_1 + k_2^{L,r} x_2 - \omega t)} + a^{S,r} \psi^{S,r} e^{i(k_1^{S,r} x_1 + k_2^{S,r} x_2 - \omega t)} \\ + a^{L,t} \psi^{L,t} e^{i(k_1^{L,t} x_1 + k_2^{L,t} x_2 - \omega t)} + a^{S,t} \psi^{S,t} e^{i(k_1^{S,t} x_1 + k_2^{S,t} x_2 - \omega t)}, \quad (3.7)$$

where  $a^{L,r}, a^{S,r}, a^{L,t}, a^{S,t} \in \mathbb{C}$  are constants to be determined from the boundary conditions,  $k_1^{L,t} = -k_1^{L,r}$  and  $k_1^{S,t} = -k_1^{S,r}$ , according to (3.4). Depending on the specific problems which are considered (e.g. semi-infinite media), only some modes may propagate in specific directions. In this case, some of the terms in

<sup>4</sup>As we will show in the following,  $k_2$ , which is the second component of the wave-number, is always supposed to be known and is given by Snell’s law when imposing boundary conditions on a given boundary.

the sum (3.7) have to be omitted. In particular, if we are considering waves propagating in the  $x_1 < 0$  half-space, then the solution to (2.1) reduces to:<sup>5</sup>

$$u(x_1, x_2, t) = a^{L,r} \psi^{L,r} e^{i(k_1^{L,r} x_1 + k_2^{L,r} x_2 - \omega t)} + a^{S,r} \psi^{S,r} e^{i(k_1^{S,r} x_1 + k_2^{S,r} x_2 - \omega t)}, \quad (3.8)$$

while if we are considering the  $x_1 > 0$  half-space, then the solution to (2.1) reduces to:

$$u(x_1, x_2, t) = a^{L,t} \psi^{L,t} e^{i(k_1^{L,t} x_1 + k_2^{L,t} x_2 - \omega t)} + a^{S,t} \psi^{S,t} e^{i(k_1^{S,t} x_1 + k_2^{S,t} x_2 - \omega t)}. \quad (3.9)$$

### 3.2 Relaxed micromorphic continuum

We start by collecting the unknown fields for the plane-strain case in a new variable:

$$v := (u_1, u_2, P_{11}, P_{12}, P_{21}, P_{22})^T. \quad (3.10)$$

The plane-wave ansatz for this unknown field reads:

$$v = \hat{\phi} e^{i(\langle k, x \rangle - \omega t)} = \hat{\phi} e^{i(k_1 x_1 + k_2 x_2 - \omega t)}, \quad (3.11)$$

where  $\hat{\phi} \in \mathbb{C}^6$  is the vector of amplitudes,  $k = (k_1, k_2)^T \in \mathbb{C}^2$  is the wave-vector<sup>6</sup> and  $\omega$  is the angular frequency. We plug this into (2.8) and get an algebraic system of the form

$$\hat{A}(k_1, k_2, \omega) \cdot \hat{\phi} = 0, \quad (3.12)$$

where  $\hat{A}(k_1, k_2, \omega) \in \mathbb{C}^{6 \times 6}$  is a matrix depending on  $k_1, k_2, \omega$  and all the material parameters of the plane-strain tetragonal relaxed micromorphic model (see A.2 for an explicit presentation of this matrix). In order for this system to have a solution other than the trivial one, we impose  $\det \hat{A} = 0$ .

The equation  $\det \hat{A} = 0$  is a polynomial of order 12 in  $\omega$  and it involves only even powers of  $\omega$ . This means that, plotting the roots  $\omega = \omega(k)$  gives 6 dispersion curves in the  $\omega - k$  plane (see Fig. 3). On the other hand, the same polynomial is of order 4 (and bi-quadratic), if regarded as a polynomial of  $k_1$  ( $k_2$  is supposed to be known when imposing boundary conditions) when setting  $L_c = 0$ . We can write the roots of the characteristic polynomial as:

$$k_1^{(1)}(k_2, \omega), \quad k_1^{(2)}(k_2, \omega), \quad k_1^{(3)}(k_2, \omega) = -k_1^{(1)}(k_2, \omega), \quad k_1^{(4)}(k_2, \omega) = -k_1^{(2)}(k_2, \omega). \quad (3.13)$$

We have verified that, plotting the two functions  $k^{(1)}(\omega) := \sqrt{(k_1^{(1)})^2 + (k_2^{(1)})^2}$  and

$k^{(2)}(\omega) := \sqrt{(k_1^{(2)})^2 + (k_2^{(2)})^2}$  gives the same diagrams as in Fig. 3. This means that each of the 2 modes  $k^{(i)}$ ,  $i = \{1, 2\}$  actually gives rise to 3 branches in the  $k - \omega$  plane.

We plug the solutions (3.13) into (3.12) and calculate the eigenvectors of  $\hat{A}$ , which we denote by:  $\hat{\phi}^{(1)}, \hat{\phi}^{(2)}, \hat{\phi}^{(3)}, \hat{\phi}^{(4)}$ . We normalize these eigenvectors, thus introducing the normal vectors

$$\phi^{(1)} := \frac{1}{|\hat{\phi}^{(1)}|} \hat{\phi}^{(1)}, \quad \phi^{(2)} := \frac{1}{|\hat{\phi}^{(2)}|} \hat{\phi}^{(2)}, \quad \phi^{(3)} := \frac{1}{|\hat{\phi}^{(3)}|} \hat{\phi}^{(3)}, \quad \phi^{(4)} := \frac{1}{|\hat{\phi}^{(4)}|} \hat{\phi}^{(4)}. \quad (3.14)$$

Considering a micromorphic medium in which all waves travel simultaneously, the solution to (2.8) is:

$$v(x_1, x_2, t) = \sum_{j=1}^4 \alpha_j \phi^{(j)} e^{i(k_1^{(j)} x_1 + k_2^{(j)} x_2 - \omega t)}, \quad (3.15)$$

where  $\alpha_j \in \mathbb{C}$  are unknown constants which will be determined from the boundary conditions,  $k_1^{(3)} = -k_1^{(1)}$  and  $k_1^{(4)} = -k_1^{(2)}$ . If, on the basis of the particular interface problem one wants to study only some waves traveling in the considered medium, then the extra waves must be omitted from the

<sup>5</sup>This choice for the sign of  $k_1$  always gives rise to a solution which verifies conservation of energy at the interface. We will show in the following, that this particular choice, which at a first instance is rather intuitive, is not always the correct one when dealing with a relaxed micromorphic medium.

<sup>6</sup>Here again, as in the case of a Cauchy medium,  $k_2$  will be fixed and given by Snell's law when imposing boundary conditions.

sum in (3.15). This means that if we are considering waves traveling in the  $x_1 > 0$  direction, then the solution to (2.8) is given by

$$v(x_1, x_2, t) = \alpha_1 \phi^{(1)} e^{i(k_1^{(1)} x_1 + k_2^{(1)} x_2 - \omega t)} + \alpha_2 \phi^{(2)} e^{i(k_1^{(2)} x_1 + k_2^{(2)} x_2 - \omega t)}, \quad (3.16)$$

while if the wave is traveling in the  $x_1 < 0$  direction, the solution to (2.8) is given by

$$v(x_1, x_2, t) = \alpha_3 \phi^{(3)} e^{i(k_1^{(3)} x_1 + k_2^{(3)} x_2 - \omega t)} + \alpha_4 \phi^{(4)} e^{i(k_1^{(4)} x_1 + k_2^{(4)} x_2 - \omega t)}. \quad (3.17)$$

## 4 Boundary Conditions

In this paper we will consider two types of interface problems: (i) a **single interface** separating a Cauchy and a relaxed micromorphic medium, both assumed to be semi-infinite and (ii) a **micromorphic slab** of finite size embedded between two semi-infinite Cauchy media. In the following, we will simply denote “single interface” and “micromorphic slab” the first and second problem, respectively.

In the single interface problem, two infinite half-spaces are occupied by two materials in perfect contact with each other. The material on the left of the interface is an isotropic classical Cauchy medium, while the material on the right is a microstructured tetragonal metamaterial modeled by the tetragonal relaxed micromorphic model (see Fig 1(a)).

In the micromorphic slab problem, two infinite half-spaces are separated by a micromorphic slab of finite width  $h$ . Three materials are thus in perfect contact with each other: the material on the left of the first interface is a classical linear elastic isotropic Cauchy medium, the material in the middle is an anisotropic relaxed micromorphic medium, while the material on the right of the second interface is again a classical isotropic Cauchy medium (see Fig. 1(b)).

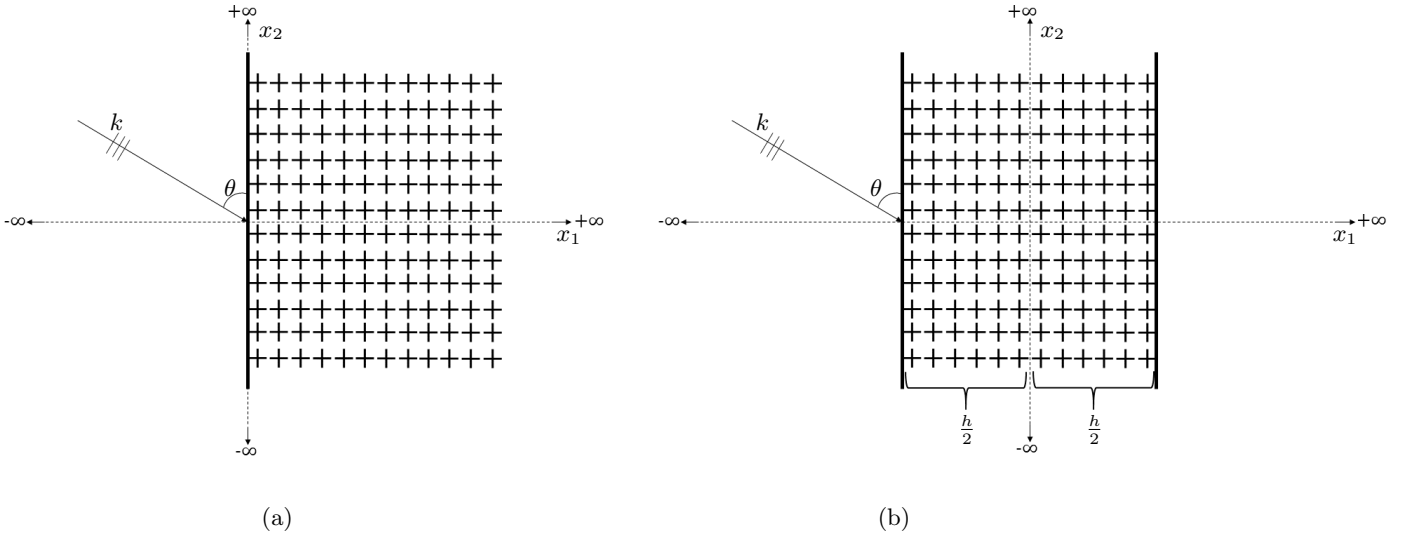


Figure 1: Panel (a): single interface separating a Cauchy medium from a relaxed micromorphic medium (both semi-infinite in the  $x_1$  direction). Panel (b): A micromorphic slab of width  $h$  between two semi-infinite elastic Cauchy media. Both configurations (a) and (b) are semi-infinite in the  $x_2$  direction.

### 4.1 Boundary conditions at an interface between a Cauchy continuum and a relaxed micromorphic continuum with vanishing characteristic length $L_c = 0$

In the particular case where  $L_c = 0$ , there are two sets of boundary conditions which have to be imposed: continuity of displacement and continuity of generalized traction (see [1, 2, 25] for more details).<sup>7</sup> For

<sup>7</sup>On the other hand, if  $L_c > 0$ , one should also impose boundary conditions on the tangent part of the micro-distortion tensor  $P$  and of the double force (see [1, 2, 25]).

the displacement, we have:

$$[[u]] = 0 \Rightarrow u^- = u^+, \quad \text{on } x_1 = 0, \quad (4.1)$$

where  $u^-$  is the macroscopic displacement on the “minus” side (the  $x_1 < 0$  half-plane, occupied by an isotropic Cauchy medium) and  $u^+$  is the macroscopic displacement on the “plus” side (the  $x_1 > 0$  half-plane, occupied by an anisotropic relaxed micromorphic medium). As for the jump of generalized traction we have:

$$t = \tilde{t}, \quad (4.2)$$

where  $t$  is the Cauchy traction on the “minus” side and  $\tilde{t}$  is the generalized traction on the “plus” side. We recall that in a Cauchy medium,  $t = \sigma \cdot \nu$ ,  $\nu$  being the outward unit normal to the surface and  $\sigma$  being the Cauchy stress tensor given by (2.2). The generalized traction for the relaxed micromorphic medium is given by

$$\tilde{t} = (\tilde{\sigma} + \hat{\sigma}) \cdot \nu, \quad \tilde{t}_i = (\tilde{\sigma}_{ij} + \hat{\sigma}_{ij}) \cdot \nu_j, \quad \text{on } x_1 = 0, \quad (4.3)$$

where  $\tilde{\sigma}, \hat{\sigma}$  are defined in (2.9).

#### 4.1.1 Continuity of macroscopic displacement and of generalized force implies conservation of energy at the interface

We have previously shown that conservation of energy for a bulk Cauchy and relaxed micromorphic medium is given by equation (2.3), where the energy flux is defined in (2.4) and (2.10), respectively. It is important to remark that the conservation of energy (2.3) has a “boundary counterpart”. This establishes that the jump of the normal part of the flux must be vanishing, or, in other words, the normal part of the flux must be continuous at the considered interface (this comes from the bulk conservation law and the use of the Gauss divergence theorem). In symbols, when considering a surface  $\Sigma$  separating two continuous media, we have

$$[[H \cdot \nu]] = 0, \quad \text{on } \Sigma. \quad (4.4)$$

We want to focus the reader’s attention on the fact that, in the framework of a consistent theory in which the bulk equations and boundary conditions are simultaneously derived by means of a variational principle, the jump conditions imposed on  $\Sigma$  necessarily imply the surface conservation of energy (4.4), as far as a conservative system is considered. We explicitly show here that this is true for an interface  $\Sigma$  separating a Cauchy medium from a relaxed micromorphic one. The same arguments, however, hold for interfaces between two Cauchy or two relaxed micromorphic media.

To that end, considering for simplicity that the interface  $\Sigma$  is located at  $x_1 = 0$  (so that its normal is  $\nu = (1, 0)^T$ ) and assuming  $L_c = 0$  we get from equation (2.10) that the normal flux computed on the “relaxed micromorphic” side is given by:

$$(H \cdot \nu)^+ := H_1^+ = -\nu^+ \cdot (\tilde{\sigma} + \hat{\sigma})^T \cdot u_{,t}^+ \quad \text{at } x_1 = 0. \quad (4.5)$$

By the same reasoning, the flux at the interface on the “Cauchy” side is computed from (2.4) and gives:

$$(H \cdot \nu)^- := H_1^- = -\nu^- \cdot \sigma \cdot u_{,t}^-. \quad (4.6)$$

Equation (4.4) can then be rewritten as:

$$-\nu^+ \cdot (\tilde{\sigma} + \hat{\sigma})^T \cdot u_{,t}^+ = -\nu^- \cdot \sigma \cdot u_{,t}^-. \quad (4.7)$$

It is clear that, given the jump conditions (4.1) and (4.2), the latter relation is automatically verified.<sup>8</sup>

As we will show in the remainder of this paper, when modeling a metamaterial’s boundary via the relaxed micromorphic model, we only need a finite number of modes in order to exactly verify boundary conditions and, consequently, surface energy conservation. This provides the most powerful simplification of the relaxed micromorphic model with respect to classical homogenization methods, in which infinite modes are needed to satisfy conservation of stress and displacement at the metamaterial’s boundary (see [39]). The first step towards the final goal of studying finite-sized complex metastructures, will be made in this paper by studying the scattering properties of a finite-sized relaxed micromorphic slab.

<sup>8</sup>An analogous calculation can be done with  $L_c > 0$ , but in that case boundary conditions on the tangent part of  $P$  and of the double force need to be used in order to automatically verify the conservation of energy on the boundary.

## 4.2 Boundary conditions for a micromorphic slab embedded between two Cauchy media

Given the macroscopic nature of the boundary conditions presented in section 4.1, they can be used to solve more complex large-scale problems, in which multiple interfaces are present. In particular, the boundary conditions to be satisfied at the two interfaces separating the slab from the two Cauchy media in Fig. 1(b), are continuity of displacement and continuity of generalized force. This means that we have four sets of boundary conditions, two on each interface. The finite slab has width  $h$  and we assume that the two interfaces are positioned at  $x_1 = -h/2$  and  $x_1 = h/2$ , respectively. The continuity of displacement conditions to be satisfied at the two interfaces of the slab are:<sup>9</sup>

$$u^- = \tilde{v}, \text{ on } x_1 = -\frac{h}{2}, \quad \tilde{v} = u^+, \text{ on } x_1 = \frac{h}{2}. \quad (4.8)$$

As for the continuity of generalized force, we have:

$$t^- = \tilde{t}, \text{ on } x_1 = -\frac{h}{2}, \quad \tilde{t} = t^+, \text{ on } x_1 = \frac{h}{2}, \quad (4.9)$$

where  $t^\pm = \sigma^\pm \cdot \nu^\pm$  are classical Cauchy tractions and  $\tilde{t}$  is again given by (4.3).

## 5 Reflection and transmission at the single interface

In this section, we study the two-dimensional, plane-strain, time-harmonic scattering problem from an anisotropic micromorphic half-space (see equations (2.8)), occupying the region  $x_1 > 0$  of Fig. 1(a). With reference to Fig. 1(a), the half-space  $x_1 < 0$  is filled with a linear elastic Cauchy continuum, governed by equation (2.1). For simplicity, we assume that the incident wave hits the interface at the origin. Considering that reflected waves only travel in the  $x_1 < 0$  Cauchy half-plane, only negative solutions for the  $k_1$ 's must be kept in equation (3.4), so that the total solution in the left half-space is

$$\begin{aligned} u^-(x_1, x_2, t) &= a^{L/S,i} \psi^{L/S,i} e^{i(\langle x, k^{L/S,i} \rangle - \omega t)} + a^{L,r} \psi^{L,r} e^{i(\langle x, k^{L,r} \rangle - \omega t)} + a^{S,r} \psi^{S,r} e^{i(\langle x, k^{S,r} \rangle - \omega t)} \\ &=: u^{L/S,i} + u^{L,r} + u^{S,r}, \end{aligned} \quad (5.1)$$

where we write L or S in the incident wave depending on whether the wave is longitudinal or shear and i and r in the exponents stand for “incident” and “reflected”. Analogously, the solution on the right half-space, which is occupied by a relaxed micromorphic medium, is<sup>10</sup>

$$v(x_1, x_2, t) = \alpha_1 \phi^{(1)} e^{i(\langle x, k^{(1)} \rangle - \omega t)} + \alpha_2 \phi^{(2)} e^{i(\langle x, k^{(2)} \rangle - \omega t)}, \quad (5.2)$$

where we have kept only terms with positive  $k_1$ 's in the solution (3.13), since transmitted waves are supposed to propagate in the  $x_1 > 0$  half-plane.<sup>11</sup>

Since the incident wave is always propagative, the polarization and wave-vectors are given by:

$$\psi^{L,i} = (\sin \theta^L, -\cos \theta^L)^T, \quad k^L = |k^L|(\sin \theta^L, -\cos \theta^L)^T, \quad (5.3)$$

$$\psi^{S,i} = (\cos \theta^S, \sin \theta^S)^T, \quad k^S = |k^S|(\sin \theta^S, -\cos \theta^S)^T, \quad (5.4)$$

where, according to (3.4),  $|k^L| = \frac{\omega}{c_L}$  and  $|k^S| = \frac{\omega}{c_S}$ , with  $c_L = \sqrt{(2\mu + \lambda)/\rho}$  and  $c_S = \sqrt{\mu/\rho}$  the longitudinal and shear speeds of propagation and  $\theta^L$  and  $\theta^S$  the angles of incidence when the wave is longitudinal or shear, respectively (see Fig. 1 and [2] for a more detailed exposition).

The continuity of displacement condition (4.1) provides us with the generalized Snell's law for the case of a Cauchy/relaxed micromorphic interface (see [2] for a detailed derivation):

$$\boxed{k_2^{L/S,i} = k_2^{L,r} = k_2^{S,r} = k_2^{(1)} = k_2^{(2)}} \quad (5.5)$$

**Generalized Snell's Law**

<sup>9</sup>We denote by  $\tilde{v}$  the first two components of the micromorphic field  $v$  defined in equation (3.11).

<sup>10</sup>We suppose here that, for the transmitted wave we have to consider only the positive solutions of (3.13). Even though this choice can seem rather intuitive, it is not the correct one since negative refraction can take place for high frequencies in order to respect conservation of energy.

<sup>11</sup>We will show in section 8 that, given the anisotropy of the relaxed micromorphic model, there exist some angles of incidence and some frequencies, for which this choice for the sign of the  $k_1$ 's is not correct, in the sense that conservation of energy (2.3) is not satisfied. In fact, for these angles of incidence and frequency intervals, we have to invert the sign of the  $k_1$ 's in order to correctly satisfy conservation of energy. This can be somehow related to what is known in the literature as negative refraction phenomena.

As for the flux, the normal outward pointing vector to the surface (the  $x_2$  axis) is  $\nu = (-1, 0)$ . This means that in expressions (2.4) and (2.10) for the fluxes, we need only take into account the first component. According to our definitions (2.4) and (2.10) (remembering that  $L_c = 0$  and that we impose the plane-strain restriction), we have

$$H_1^- = -u_{i,t} \sigma_{i1}, \quad H_1^+ = -v_{i,t} (\tilde{\sigma}_{i1} + \hat{\sigma}_{i1}), \quad i = 1, 2. \quad (5.6)$$

Having calculated the “transmitted” flux, we can now look at the reflection and transmission coefficients for the case of a Cauchy/relaxed micromorphic interface. We define<sup>12</sup>

$$J^i = \frac{1}{T} \int_0^T H^i(x, t) dt, \quad J^r = \frac{1}{T} \int_0^T H^r(x, t) dt, \quad J^t = \frac{1}{T} \int_0^T H^t(x, t) dt, \quad (5.7)$$

where  $T$  is the time period of the considered harmonic waves,  $H^i = H_1^-(u^{L/S,i})$ ,  $H^r = H_1^-(u^{L,r} + u^{S,r})$  and  $H^t = H_1^+(v)$ , with  $H_1^+$  and  $H_1^-$  defined in (5.6). Then the reflection and transmission coefficients are

$$\mathcal{R} = \frac{J^r}{J^i}, \quad \mathcal{T} = \frac{J^t}{J^i}. \quad (5.8)$$

Since the system is conservative, we must have that  $\mathcal{R} + \mathcal{T} = 1$ .

## 6 Reflection and transmission at a relaxed micromorphic slab

As pointed out, in this case there are three media: the first Cauchy half-space, the anisotropic relaxed micromorphic slab and the second Cauchy half-space. The two Cauchy half-spaces are denoted by  $-$  and  $+$ , while the quantities considered in the slab have their own notation.

The solution on the first Cauchy half space is given, as in the case of a single interface, by

$$u^-(x_1, x_2, t) = a^{L/S,i} \psi^{L/S,i} e^{i(\langle x, k^{L/S,i} \rangle - \omega t)} + a^{L,r} \psi^{L,r} e^{i(\langle x, k^{L,r} \rangle - \omega t)} + a^{S,r} \psi^{S,r} e^{i(\langle x, k^{S,r} \rangle - \omega t)}. \quad (6.1)$$

In the case of a relaxed micromorphic slab, when solving the eigenvalue problem we must select and keep all the roots for  $k_1$ , as given in (3.13), both positive and negative. This is due to the fact that there are waves which transmit in the micromorphic part from the first interface ( $x_1 = -h/2$ ), upon which the incident wave hits and waves which reflect on the second interface ( $x_1 = h/2$ ). This means that the solution of the PDEs in the slab is

$$v(x_1, x_2, t) = \alpha_1 \phi^{(1)} e^{i(\langle x, k^{(1)} \rangle - \omega t)} + \alpha_2 \phi^{(2)} e^{i(\langle x, k^{(2)} \rangle - \omega t)} + \alpha_3 \phi^{(3)} e^{i(\langle x, k^{(3)} \rangle - \omega t)} + \alpha_4 \phi^{(4)} e^{i(\langle x, k^{(4)} \rangle - \omega t)}, \quad (6.2)$$

where  $k_1^{(1)} = -k_1^{(3)}$  and  $k_1^{(2)} = -k_1^{(4)}$  (see section 3.2). Finally, the solution on the right Cauchy half-space is

$$u^+(x_1, x_2, t) = a^{L,t} \psi^{L,t} e^{i(\langle x, k^{L,t} \rangle - \omega t)} + a^{S,t} \psi^{S,t} e^{i(\langle x, k^{S,t} \rangle - \omega t)}. \quad (6.3)$$

The continuity of displacement conditions (4.8) again imply a generalized form of Snell’s law for the case of the micromorphic slab:

$$k_2^{L/S,i} = k_2^{L,r} = k_2^{S,r} = k_2^{(1)} = k_2^{(2)} = k_2^{(3)} = k_2^{(4)} = k_2^{L,t} = k_2^{S,t}. \quad (6.4)$$

**Generalized Snell’s Law in a micromorphic slab**

In order to define the reflection and transmission coefficients in the case of the anisotropic slab, we follow the same reasoning as for the single interface. However, in this case, the transmitted flux is defined as the flux on the right of the second interface, which is occupied by an isotropic Cauchy medium.

In this case, the reflected flux is evaluated at  $x_1 = -h/2$  and the transmitted flux at  $x_1 = h/2$ . Both the reflected and the transmitted fields propagate in isotropic Cauchy media, so that the quantities  $J^i, J^r, J^t$  defined in (5.7) are given by (see [2])

$$J_{\text{slab}}^i = \frac{1}{2} \text{Re} \left( \left[ (2\mu^- + \lambda^-) \left| \psi_1^{j,i} \right|^2 k_1^{j,i} + \lambda^- \left( \psi_1^{j,i} \right)^* \psi_2^{j,i} k_2^{j,i} + \mu^- \left( \psi_1^i \left( \psi_2^{j,i} \right)^* k_2^{j,i} + \left| \psi_2^{j,i} \right|^2 k_1^{j,i} \right) \right] \left| a^{j,i} \right|^2 \omega \right), \quad (6.5)$$

<sup>12</sup>In order to easily compute these coefficients in the numerical implementation of the code, we employ Lemma 1 given in Appendix A.3.

$$J_{\text{slab}}^r = \sum_{j \in \mathcal{J}} \frac{1}{2} \text{Re} \left( \left[ (2\mu^- + \lambda^-) |\psi_1^{j,r}|^2 k_1^{j,r} + \lambda^- (\psi_1^{j,r})^* \psi_2^{j,r} k_2^{j,i} + \mu^- (\psi_1^{j,r} (\psi_2^{j,(2)})^* k_2^{j,i} |\psi_2^{j,r}|^2 k_1^{j,r}) \right] |a^{j,r}|^2 \omega \right), \quad (6.6)$$

$$J_{\text{slab}}^t = \sum_{j \in \mathcal{J}} \frac{1}{2} \text{Re} \left( \left[ (2\mu^+ + \lambda^+) |\psi_1^{j,t}|^2 k_1^{j,t} + \lambda^+ (\psi_1^{j,t})^* \psi_2^{j,t} k_2^{j,i} + \mu^+ (\psi_1^{j,t} (\psi_2^{j,t})^* k_2^{j,i} + |\psi_2^{j,t}|^2 k_1^{j,t}) \right] |a^{j,t}|^2 \omega \right), \quad (6.7)$$

where,  $\mathcal{J} \in \{L, S\}$ ,  $a^{j,i}, a^{j,r}, a^{j,t} \in \mathbb{C}$  and  $\psi^{j,i}, \psi^{j,(2)}, \psi^{j,t} \in \mathbb{C}^2$  with  $\mathcal{J} \in \{L, S\}$ , are the amplitudes and polarization vectors for incident, reflected and transmitted waves, respectively (see also equation (3.6)),  $\mu^-, \lambda^-$  and  $\mu^+, \lambda^+$  are the Lamé parameters of the left and right Cauchy half-spaces, respectively.

So, the reflection and transmission coefficients for the slab are

$$\mathcal{R}_{\text{slab}} = \frac{J_{\text{slab}}^r}{J_{\text{slab}}^i}, \quad \mathcal{T}_{\text{slab}} = \frac{J_{\text{slab}}^t}{J_{\text{slab}}^i}. \quad (6.8)$$

Since the system is conservative, we must have  $\mathcal{R}_{\text{slab}} + \mathcal{T}_{\text{slab}} = 1$ .

## 7 Reflective properties of a micro-structured slab

Here, we consider the scattering of in-plane elastic waves from a slab containing cross like holes drilled in an isotropic elastic material (see Fig. 2(a)). The holes in the micro-structured slab are arranged according to a truncated square lattice, i.e. a finite number  $N$  of cells in the  $x_1$  direction and an infinite number of cells in the  $x_2$  direction.

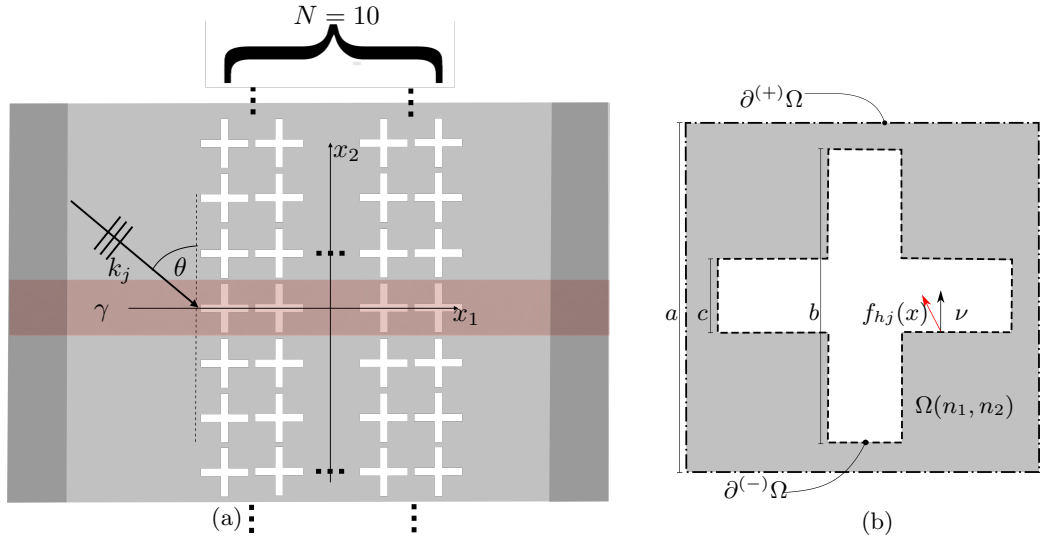


Figure 2: Panel (a) is a schematic representation of a slab of cross like-holes which is finite in the  $x_1$ -direction ( $N = 10$  number of unit cells) and periodic in the  $x_2$ -direction. The red shadows represent the finite element domain  $\gamma$  where the scattering problem is set up and solved. The domain  $\gamma$  contains two perfectly matched layers (darker red regions at the sides of the rectangular domain  $\gamma$ ). Panel (b) is a schematic representation of a unit cell  $\Omega(n_1, n_2)$ , for a generic pair of integers  $(n_1, n_2)$ . The inner boundary  $\partial^{(-)}\Omega(n_1, n_2)$  (dashed black line), the outer boundary  $\partial^{(+)}\Omega(n_1, n_2)$  (dot-dashed black line), and the normal and traction vectors along  $\partial^{(-)}\Omega(n_1, n_2)$  (black and red arrow lines, respectively) are also shown.

We consider an incident time-harmonic plane wave

$$u^{j,i}(x, t) = \bar{u}^{j,i}(x) e^{-i\omega t} = d^j e^{i\langle k^j, x \rangle - i\omega t}, \quad (7.1)$$

where the index  $j \in \{L, S\}$  denotes longitudinal and shear waves, respectively. Accordingly,  $k^j = \omega/c_j (\sin \theta, -\cos \theta, 0)^T$ , with  $j \in \{L, S\}$  and  $\theta$  the angle of incidence,  $c_L = \sqrt{(\lambda_{\text{Al}} + 2\mu_{\text{Al}})/\rho_{\text{Al}}}$  and  $c_S = \sqrt{\mu_{\text{Al}}/\rho_{\text{Al}}}$  are the longitudinal and shear wave speeds for aluminum. The Lamé parameters of aluminum are  $\lambda_{\text{Al}} = 5.11 \times 10^{10}$  Pa and  $\mu_{\text{Al}} = 2.63 \times 10^{10}$  Pa, and the density of aluminum is  $\rho_{\text{Al}} = 2700$  Kg/m<sup>3</sup>. The Lamé parameters define uniquely the fourth order stiffness tensor  $\mathbb{C}_{\text{Al}}$ , whose

Voigt representation is

$$\tilde{\mathbb{C}}_{\text{Al}} = \begin{pmatrix} 2\mu_{\text{Al}} + \lambda_{\text{Al}} & \lambda_{\text{Al}} & \star & 0 & 0 & 0 \\ \lambda_{\text{Al}} & 2\mu_{\text{Al}} + \lambda_{\text{Al}} & \star & 0 & 0 & 0 \\ \star & \star & \star & 0 & 0 & 0 \\ 0 & 0 & 0 & \star & 0 & 0 \\ 0 & 0 & 0 & 0 & \star & 0 \\ 0 & 0 & 0 & 0 & 0 & \mu_{\text{Al}} \end{pmatrix}, \quad (7.2)$$

where the stars denote the components which do not intervene in the plane-strain case. In equation (7.1) we have introduced the polarization vectors  $d^j$ ,  $j \in \{L, S\}$  of amplitude  $d_0$  for longitudinal and shear waves, defined as  $d^L = d_0(\sin \theta, -\cos \theta, 0)^T$  and  $d^S = d_0(\cos \theta, \sin \theta, 0)^T$ , respectively. The scattering problem in terms of the elastic plane-strain field  $u^j \equiv u^j(x, t)$ ,  $j \in \{L, S\}$ , in the micro-structured material, according to linear elasticity, can be written as

$$\begin{cases} \rho_{\text{Al}} u_{,tt}^j = \text{Div}(\mathbb{C}_{\text{Al}} \text{sym} \nabla u^j), & x \in \Omega_0(n_1, n_2) \\ f(u^j) = 0, & x \in \partial^{(-)}\Omega(n_1, n_2), \quad \forall n_1 \in \{1, \dots, N\} \quad \text{and} \quad \forall n_2 \in \mathbb{Z}, \end{cases} \quad (7.3)$$

where we have introduced the traction vectors

$$f(u^j) = (\mathbb{C}_{\text{Al}} \text{sym} \nabla u^j) \cdot \nu, \quad j \in \{L, S\}, \quad (7.4)$$

$\nu$  being the normal unit vector (see black arrow line in Fig. 2(b)) to the cross-like holes boundaries  $\partial^{(-)}\Omega(n_1, n_2)$  and where we denote by  $\Omega_0$  the part of the domain  $\Omega$ , which is non-empty (occupied by aluminum). The elastic field in (7.3) can be written according to the scattering time-harmonic ansatz

$$u^j(x, t) = (\bar{u}^{j,i}(x) + \bar{u}^{j,\text{sc}}(x)) e^{-i\omega t}, \quad j \in \{L, S\}, \quad (7.5)$$

where  $\bar{u}^{j,i}$  has been introduced in equation (7.1) and  $\bar{u}^{j,\text{sc}}$  is the so-called scattered solution. By linearity of the traction vector (7.4), and using equation (7.5), we obtain

$$f(u^j(x, t)) = [f(\bar{u}^{j,i}(x)) + f(\bar{u}^{j,\text{sc}}(x))] e^{-i\omega t} = 0, \quad j \in \{L, S\}. \quad (7.6)$$

Using the fact that  $u^{j,i}(x, t)$  is a solution of the PDE in equation (7.3), together with equation (7.6), the PDEs system (7.3) can be rewritten in a time-harmonic form with respect to the field  $u^{j,\text{sc}}(x)$ , as:

$$\begin{cases} -\omega^2 \rho_{\text{Al}} \bar{u}^{j,\text{sc}} = \text{Div}(\mathbb{C}_{\text{Al}} \text{sym} \nabla \bar{u}^{j,\text{sc}}), & x \in \Omega_0 \\ f(\bar{u}^{j,\text{sc}}) \equiv (\mathbb{C}_{\text{Al}} \text{sym} \nabla \bar{u}^{j,\text{sc}}) \cdot \nu = -f(\bar{u}^{j,i}), & x \in \partial^{(-)}\Omega(n_1, n_2), \quad \forall n_1 \in \{1, \dots, N\} \quad \text{and} \quad \forall n_2 \in \mathbb{Z}, \end{cases} \quad (7.7)$$

with  $j \in \{L, S\}$  and where we have canceled out time-harmonic factors. The analytical expressions for the boundary conditions for the scattered field (see right-hand side of the boundary conditions in equation (7.7)) are given component-wise as:

$$\begin{aligned} f(\bar{u}^{j,i}) \cdot e_1 &:= f_v^j(x) = (\mathbb{C}_{\text{Al}} \text{sym} \nabla \bar{u}^{j,i}) \cdot e_1 \\ &= \frac{i\omega\rho}{c_j} \left\{ \left[ c_L^2 \sin \theta d_1^{j,i} - (c_L^2 - 2c_S^2) \cos \theta d_2^{j,i} \right] e_1 + c_S^2 \left[ -\cos \theta d_1^{j,i} + \sin \theta d_2^{j,i} \right] e_2 \right\} e^{i\langle k^{j,i}, x \rangle}, \end{aligned} \quad (7.8)$$

with  $j \in \{L, S\}$  for vertical boundaries of  $\partial^{(-)}\Omega(n_1, n_2)$  with normal vector parallel to  $e_1$  (see Fig. 2(b)). Similarly, for vertical boundaries with normal vector anti-parallel to  $e_1$  we have  $f(\bar{u}^{j,i}) = -f_v^j(x)$ . In addition, for horizontal boundaries in  $\partial^{(-)}\Omega(n_1, n_2)$  whose normal vector is parallel to  $e_2$  we have:

$$\begin{aligned} f(\bar{u}^{j,i}) \cdot e_2 &:= f_h^j(x) = (\mathbb{C}_{\text{Al}} \text{sym} \nabla \bar{u}^{j,i}) \cdot e_2 \\ &= \frac{i\omega\rho}{c_j} \left\{ \left[ (c_L^2 - 2c_S^2) \sin \theta d_1^{j,i} - c_L^2 \cos \theta d_2^{j,i} \right] e_2 + c_S^2 \left[ -\cos \theta d_1^{j,i} + \sin \theta d_2^{j,i} \right] e_1 \right\} e^{i\langle k^{j,i}, x \rangle}, \end{aligned} \quad (7.9)$$

with  $j \in \{L, S\}$ . Similarly, for vertical boundaries with normal vector anti-parallel to  $e_2$  we have  $f(\bar{u}^{j,i}) = -f_h^j(x)$ .

## 7.1 Bloch-Floquet conditions

We recall that the primitive vectors of a square lattice are defined as:

$$a_1 = a e_1, \quad \text{and} \quad a_2 = a e_2, \quad (7.10)$$

where  $a$  is the side of the unit-cell (see Fig. 2(b)). Since the scatterers (i.e. the cross-like holes) are periodic in the  $x_2$ -direction, the displacement field in equation (7.5) satisfies Bloch-Floquet boundary conditions

$$\bar{u}^{j,\text{sc}}(x + n_2 a_2) = e^{in_2 k_2 a} \bar{u}^{j,\text{sc}}(x), \quad \text{for } x \in \gamma, \quad \text{and } n_2 \in \mathbb{Z}, \quad (7.11)$$

where  $k_2$  is the component along the  $x_2$ -direction of the wave vector  $k$ . The value of  $k_2$  is known and should be equal, given the considered geometry represented in Fig. 2(a), to the second component of the wave vector of the incident wave. This requirement is essential in order to construct a solution which satisfies the prescribed boundary conditions within a micro-structured medium which is periodic in one dimension, i.e. in a layered micro-structured medium (see e.g. [33]). This, of course, is the well known Snell's law governing the refraction of waves at the interface between two half-spaces with different material parameters (see the book by Leckner [16] for a mathematical introduction encompassing several physical scenarios). As it is customary in Floquet theory of PDEs with periodic coefficients, we can obtain the solution of the PDEs system (7.7), by solving the problem in its period (i.e. the red strip in Fig. 2(a) here denoted as  $\gamma$ ) provided that the Bloch-Floquet condition (7.11) on the scattered field is satisfied.

Although the  $x_1$  extension of the domain  $\gamma$  is infinite in our model problem, in the finite-element implementation of the boundary value problem we are of course restricted to finite computational domains. In order to annihilate the reflection from the sides of  $\gamma$  with constant  $x_1$ , we use perfectly matched layers [6] away from the microstructure.

## 7.2 Reflectance

The time-averaged Poynting vector associated with a 2D time-harmonic displacement field  $u(x, t) = \bar{u}(x) e^{-i\omega t}$  is defined as [2, 3]

$$F = -\frac{\omega}{2} \text{Re}(i\sigma \cdot u^*), \quad (7.12)$$

where “ $*$ ” denotes complex conjugation and  $\sigma = \mathbb{C}_{\text{Al}} \text{sym} \nabla u$  is the Cauchy stress tensor associated with the elastic field  $u$ . From equation (7.12), and using equation (7.1), it follows that the energy flux associated with the incident displacement field (7.1) is

$$F^{j,\text{i}} = \frac{1}{2} \rho c_j |d^{j,\text{i}}|^2 \frac{k^{j,\text{i}}}{|k^{j,\text{i}}|}, \quad j \in \{L, S\}. \quad (7.13)$$

Similarly, we define the flux  $F^{j,\text{sc}}$  of the scattered field to be as in equation (7.12) with  $u(x, t) = \bar{u}^{j,\text{sc}}(x) e^{-i\omega t}$ , where  $\bar{u}^{j,\text{sc}}$  is the solution of the PDEs system (7.7)). The reflectance, i.e. the ratio of reflected energy and incident energy passing through a vertical line of length  $a$ , is

$$\begin{aligned} \mathcal{R}^j &= \frac{1}{\langle F^{j,\text{i}}, e_1 \rangle} \frac{1}{a} \int_{-a/2}^{a/2} \langle F^{j,\text{sc}} |_{x_1 \ll -aN/2}, e_1 \rangle dx_2, \\ &= \frac{2}{\rho c_j |d^{j,\text{i}}|^2 \sin(\theta)} \frac{1}{a} \int_{-a/2}^{a/2} \langle F^{j,\text{sc}} |_{x_1 \ll -aN/2}, e_1 \rangle dx_2, \quad j \in \{L, S\}. \end{aligned} \quad (7.14)$$

The reflectance associated with incident shear waves ( $\mathcal{R}^S$ ) differs from that associated with incident longitudinal waves ( $\mathcal{R}^L$ ). The Poynting vector is evaluated at a given  $x_1 \ll -aN/2$  away from the slab to avoid the contribution from the near elastic field close to the microstructure. Provided the condition  $x_1 \ll -aN/2$  is satisfied, we have verified that the reflectance (7.14) does not depend on the exact value of  $x_1$ .

## 8 Results and discussion

In this section we present the comparison between the refractive behavior of the finite metamaterial's slab, as modeled in Comsol (see Fig.2) and the relaxed micromorphic model (see Fig. 1). We also provide the results concerning the relaxed micromorphic single interface, which will be seen as an average behavior with respect to the micromorphic slab of finite size. To this end, we chose the material parameters of the relaxed micromorphic model as in Table 1.

$\lambda_e$	$\mu_e$	$\mu_e^*$	$\lambda_{\text{micro}}$	$\mu_{\text{micro}}$	$\mu_{\text{micro}}^*$	$\mu_c$	$L_c$	$\lambda_{\text{macro}}$	$\mu_{\text{macro}}$	$\mu_{\text{macro}}^*$
[GPa]	[GPa]	[GPa]	[GPa]	[GPa]	[GPa]	[GPa]	[m]	[GPa]	[GPa]	[GPa]
-0.77	17.34	0.67	5.98	8.93	8.33	$2.2 \cdot 10^{-3}$	0	1.74	5.89	0.62
$\rho$	$\eta_1$	$\eta_2$	$\eta_3$	$\eta_1^*$	$\bar{\eta}_1$	$\bar{\eta}_2$	$\bar{\eta}_3$	$\bar{\eta}_1^*$		
[kg/m <sup>3</sup> ]	[kg/m]	[kg/m]	[kg/m]	[kg/m]	[kg/m]	[kg/m]	[kg/m]	[kg/m]	[kg/m]	[kg/m]
1485	$9.5 \cdot 10^{-5}$	$1 \cdot 10^{-7}$	$0.86 \cdot 10^{-5}$	$3.27 \cdot 10^{-5}$	$10^{-4}$	$2 \cdot 10^{-4}$	$8 \cdot 10^{-8}$	$10^{-5}$		

Table 1: Summary of the numerical values for the elastic (top) and inertia (bottom) parameters of the tetragonal relaxed micromorphic model in the 2D plane-strain case. The macroscopic parameters of the resulting homogenized Cauchy material (see [2, 10]) are also provided (top right).

The choice of the metamaterial parameters is made according to the procedure presented in [10], which allows to determine the parameters of the relaxed micromorphic model on a specific metamaterial by an inverse approach. This fitting procedure is based on the determination of the elastic parameters of the relaxed micromorphic model via numerical static tests on the unit cell and of the remaining inertia parameters via a simple inverse fitting of the dispersion curves on the analogous dispersion patterns as obtained by Bloch-Floquet analysis (see [10] for details). The fitting of the bulk dispersion curves for the periodic metamaterial, whose unit cell is shown in Fig. 2(b), is presented in Fig. 3.

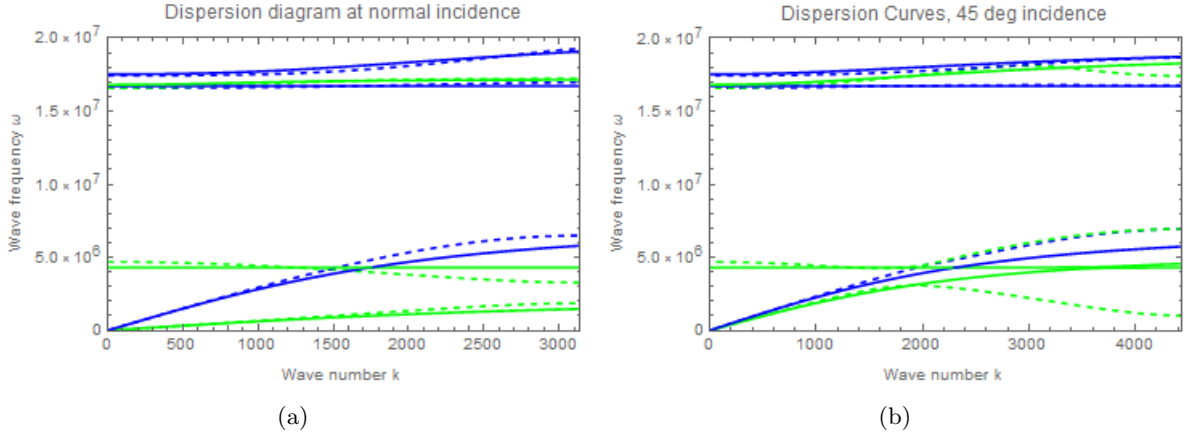


Figure 3: Dispersion diagrams for normal (a) and 45 degrees (b) incidence. The solid curves are obtained via the tetragonal anisotropic relaxed micromorphic model, while the dashed curves are issued by Bloch-Floquet analysis. In panel (a), green color stands for modes which are mostly activated by a shear incident wave, while blue color indicates modes which are mostly activated by a longitudinal incident wave. This uncoupling between L and S activated modes at normal incidence is analytically checked in the relaxed micromorphic model and only approximate for Bloch-Floquet modes. In panel (b), we keep the same coloring, but all curves are coupled together, which means that L and S incident waves may simultaneously activate all modes.

We checked that a sort of distinction between modes which are activated by an L or S incident wave can be made for an incident wave which is orthogonal to the interface. This is exactly true for the relaxed micromorphic model, but an analogous trend can be found for Bloch-Floquet modes at least for the lower frequency modes (before the band-gap). The uncoupling between L and S activated modes is

present only for  $\theta = 0$  (and, by symmetry,  $\theta = \pi/2$ ), but is lost for any other direction of propagation. In general, for any given frequency, all modes which are pertinent at that frequency may be simultaneously activated by an L or S incident wave (excluding the particular case of normal incidence). Nevertheless, we will show that this uncoupling hypothesis can be retained with little error for angles of incidence which are close to normal incidence.

Once the bulk properties of the considered metamaterial, as modeled by the relaxed micromorphic model, have been established, they can be used to study the scattering problems presented before.

## 8.1 Scattering at a relaxed micromorphic slab

We start by presenting the reflection coefficient of the relaxed micromorphic slab as a function of the frequency for two fixed directions of propagation of the incident wave ( $\theta = \frac{\pi}{2}$  and  $\theta = \frac{\pi}{4}$ ) and for both longitudinal and shear incident waves.

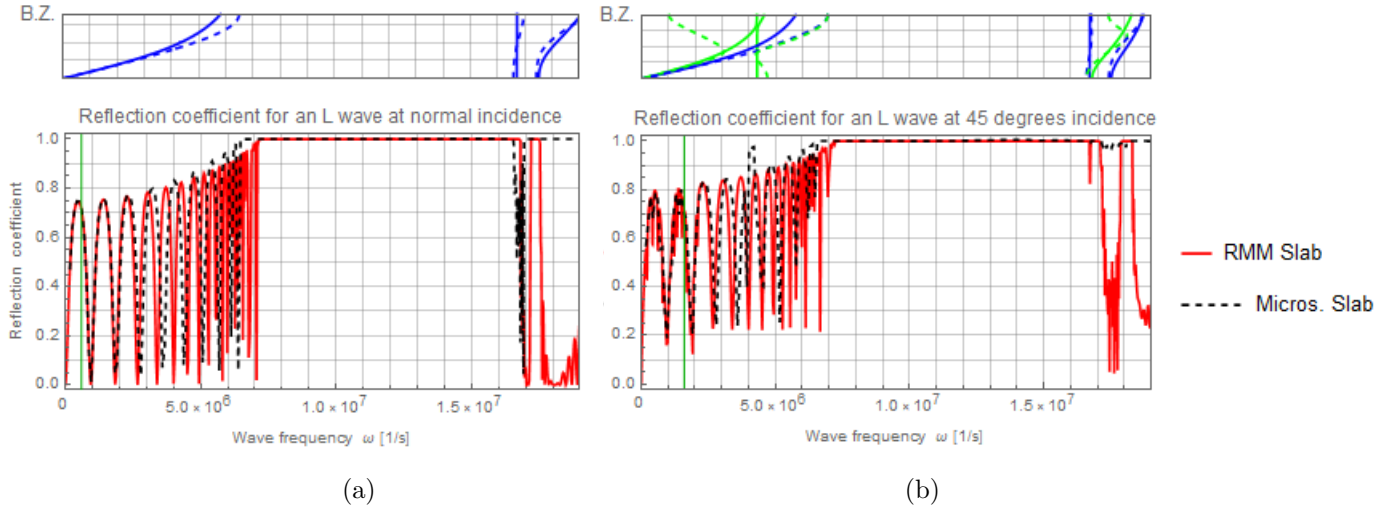


Figure 4: Reflection coefficient at the relaxed micromorphic slab for an incident L wave and for two directions of propagation  $\theta = \pi/2$  (normal incidence) (a) and  $\theta = \pi/4$  (b). The red curve is generated by the analytical tetragonal relaxed micromorphic model and the black dashed line indicates the microstructured model. The green vertical lines denote the long-wave limit, below which the relaxed micromorphic model is equivalent to a homogenized Cauchy model. The dispersion diagrams for  $\theta = \pi/2$  and  $\theta = \pi/4$ , given in Fig. 3 are also rotated and displayed on the top of each picture to allow for a better interpretation of results.

Figure 4 shows the behavior of the reflection coefficient for the considered microstructured slab in the case of a longitudinal incident wave and for normal incidence (Fig. 4(a)) as well as for incidence at  $45^\circ$  (Fig. 4(b)). The black dashed line is the solution issued via the microstructured model obtained by coding all the details of the unit cell presented in section 7. The red continuous line is obtained by solving the relaxed micromorphic problem presented in section 6, using the software Mathematica.

It is immediately evident that the relaxed micromorphic model is able to capture the overall behavior of the reflection coefficient for a very wide range of frequencies. More particularly, for lower frequencies and up to the band-gap region, oscillations of the reflection coefficient due to the finite size of the slab are observed in both models. The band-gap region is also correctly described and corresponds to the frequency interval for which complete reflection ( $\mathcal{R} = 1$ ) is observed.

After the band-gap region, a characteristic frequency can be identified corresponding to which almost complete transmission occurs. This phenomenon is related to internal resonances at the level of the microstructure. It is easy to see that the relaxed micromorphic model is able to correctly describe also the internal resonance phenomenon. The internal resonance is clearly visible in both the discrete and the relaxed micromorphic model at normal incidence. It is, however, lost in the discrete simulation at  $45^\circ$  notwithstanding the presence of a zero group velocity mode in both models. Similar arguments can be carried out for an S incident wave with reference to Fig. 5.

In addition to the comments carried out for an L incident wave, we remark in Fig. 5(a) the presence of a spurious internal resonance in the lower part of the band-gap for the relaxed micromorphic model. This spurious resonance can be eliminated by activating the non-locality of the model by setting  $L_c > 0$ . In this case, the moderate transmission present in Fig. 5(a) before the band-gap can be reproduced. More

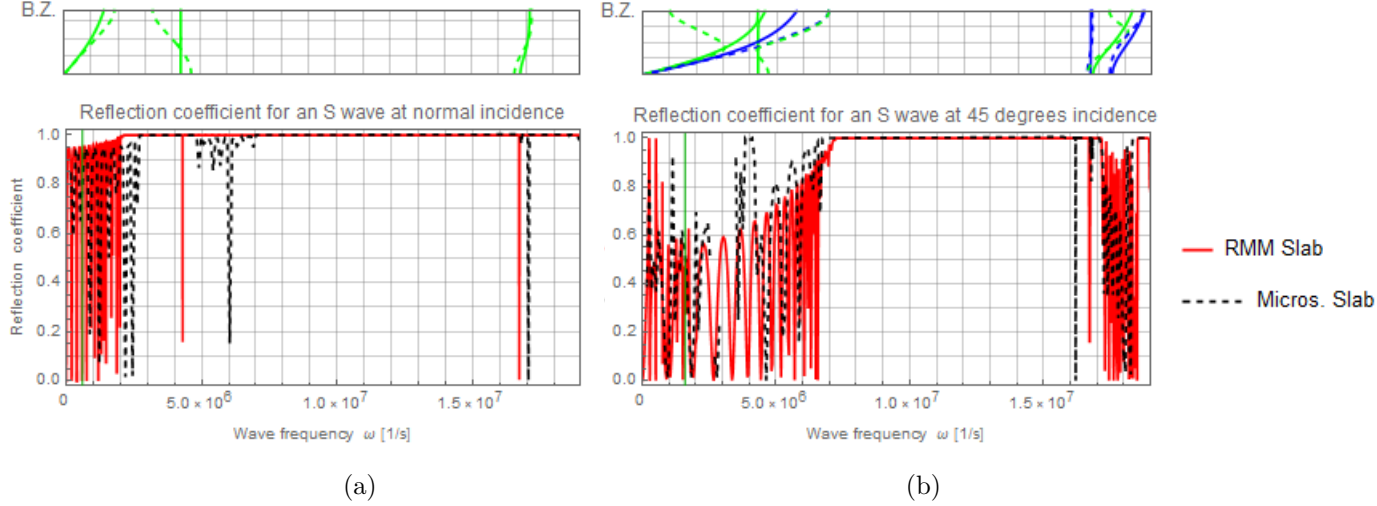


Figure 5: Reflection coefficient at the relaxed micromorphic slab for an incident S wave and for two directions of propagation  $\theta = \pi/2$  (normal incidence) (a) and  $\theta = \pi/4$  (b). The red curve is generated by the analytical tetragonal relaxed micromorphic model and the black dashed line indicates the microstructured model. The green vertical lines denote the long-wave limit, below which the relaxed micromorphic model is equivalent to a homogenized Cauchy model. The dispersion diagrams for  $\theta = \pi/2$  and  $\theta = \pi/4$ , given in Fig. 3 are also rotated and displayed on the top of each picture to allow for a better interpretation of results.

details about non-localities will be given in forthcoming papers. This moderate transmission observed in the microstructured simulations are due to the imperfect uncoupling of the S (green) modes from the L (blue) acoustic mode in the Bloch-Floquet dispersion diagram. Thus, there exist some small frequency ranges, for which the L acoustic mode can be activated also by an S incident wave. The associated transmission remains very small.

At this point, in order to fully present the potentialities of the relaxed micromorphic model, we depict in Figures 6 and 7 the transmission coefficient ( $\mathcal{T} = 1 - \mathcal{R}$ ) as a function of both the angle and frequency of the longitudinal incident wave for both the relaxed micromorphic and the microstructured models.

Figure 6 shows the broadband transmission coefficient's behavior for an L incident wave as a function of the frequency and angle of incidence. We observe an excellent agreement between the continuous and discrete simulation for frequencies lower than the band-gap. Transmission is principally allowed by the blue acoustic mode for all directions of propagation. Even if there exists some coupling at non-orthogonal incidence with the other lower frequency modes, the blue acoustic mode is the one which is predominantly activated by an L incident wave and it is, to a big extent, responsible for the transmission across the metamaterial slab. The band-gap region is also correctly described. The validation of the fitting performed on higher frequencies was impossible due to the difficulty of establishing the convergence of the microstructured simulations with the semi-analytical results of relaxed micromorphic model this issue deserves deeper investigations and will be left for forthcoming works.

Figure 7 depicts the analogous results for an S incident wave. For frequencies lower than the band-gap, we observe once again an excellent agreement between the discrete and continuous simulations for all angles of incidence.

We also remark additional interesting phenomena. Firstly, for smaller angles of incidence, we see that the band-gap region extends to lower frequencies. This is related to the previously discussed acoustic mode uncoupling, which is observed for angles close to normal incidence. A shear incident wave mostly activates the green acoustic mode (see Fig. 3) which is almost entirely responsible for the propagation pattern. Since the blue acoustic mode is not activated for angles close to normal incidence, the bottom band-gap limit is consequently lower compared to the case of an L incident wave.

A first threshold value of the angle of incidence exists (around  $5\pi/24$ ), for which the two acoustic modes start to couple and energy starts being transmitted. More remarkably, a second threshold value of the incident angle exists (around  $\pi/3$ ), for which the amount of transmission suddenly increases, approaching a total transmission pattern. This is due to a stronger coupling between the two acoustic modes which are activated by an S incident wave for incident angles beyond the second threshold. This impressive pattern is clearly associated to the tetragonal symmetry of the metamaterial: the need for introducing “generalized classes of symmetry” in an enriched continuum environment is now evident.

The investigations for higher frequencies will be discussed in forthcoming works.

We deduce that the agreement is very satisfactory for all the considered angles (going from normal incidence to incidence almost parallel to interface) and for the considered range of frequencies. This fact corroborates the hypothesis, which has been made according to Neumann's principle and which states that the class of symmetry of the metamaterial at the macroscopic scale is the same as the symmetry of the unit cell (tetragonal symmetry in this case).

We conclude this section by pointing out that the simulations performed to obtain Figures 6 and 7 took less than 1 hour for the relaxed micromorphic model and 3 weeks for the discrete model. Both computations were made with 200 points in the frequency range and for 90 angles.

This tremendous gain in computational time underlines the usefulness of an enriched continuum model versus a discrete one for the description of the mechanical behavior of finite-size metamaterials structures. Metamaterial characterization through the relaxed micromorphic model opens the way to effective FEM implementation of other morphologically complex metastructures.

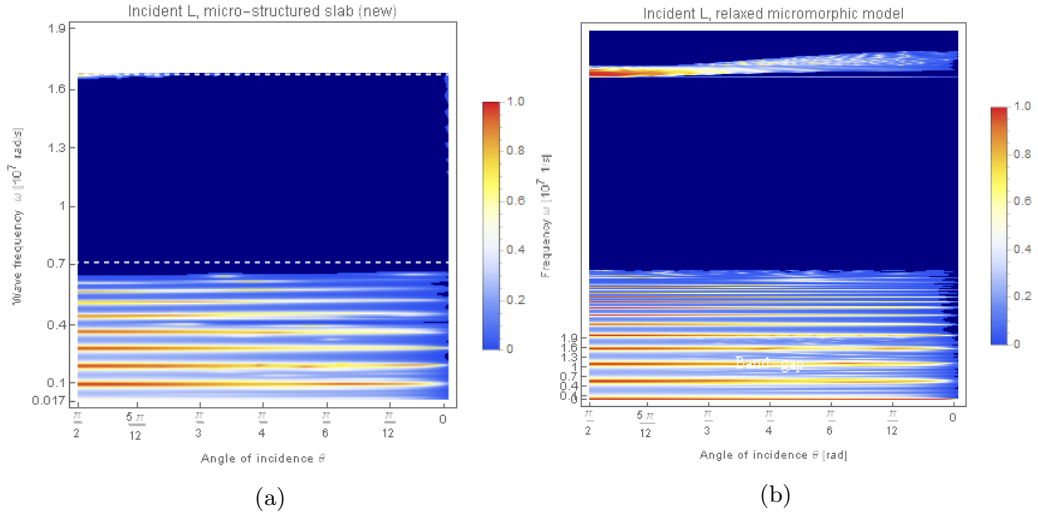


Figure 6: Transmission coefficient of the metamaterial slab as a function of the angle of incidence  $\theta$  and of the wave-frequency  $\omega$  for an incident L wave. Panel (a) depicts the microstructured simulations, while panel (b) the analytical relaxed micromorphic model. The origin coincides with normal incidence ( $\theta = \pi/2$ ), while the angle of incidence decreases towards the right until it reaches the value  $\theta = 0$ , which corresponds to the limit case where the incidence is parallel to the interface. The band-gap region is highlighted by two dashed horizontal lines, where, as expected, we observe no transmission. The dark blue zone shows that no transmission takes place, while the gradual change from dark blue to red shows the increase of transmission, red being total transmission.

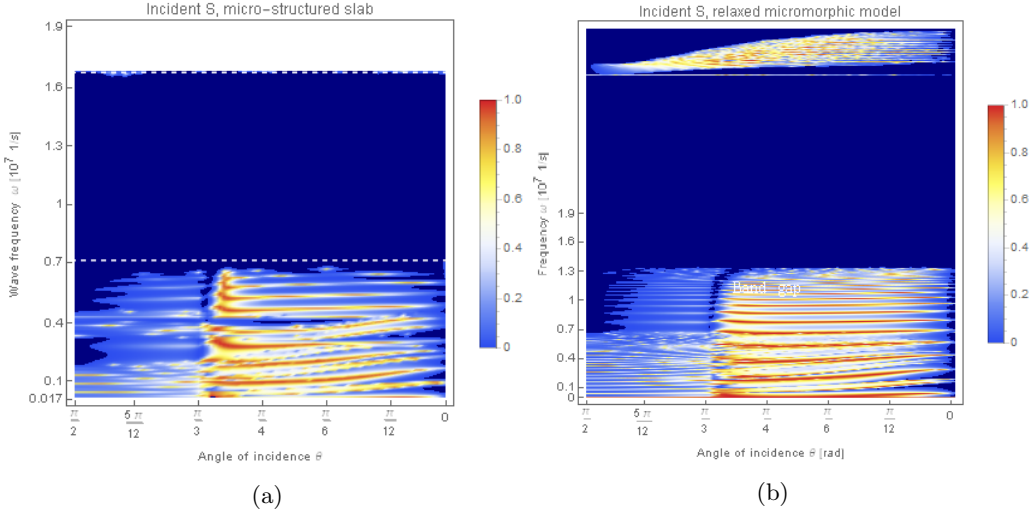


Figure 7: Transmission coefficient of the metamaterial slab as a function of the angle of incidence  $\theta$  and of the wave-frequency  $\omega$  for an incident S wave. Panel (a) depicts the microstructured simulations, while panel (b) the analytical relaxed micromorphic model. The origin coincides with normal incidence ( $\theta = \pi/2$ ), while the angle of incidence decreases towards the right until it reaches the value  $\theta = 0$ , which corresponds to the limit case where the incidence is parallel to the interface. The band-gap region is highlighted by two dashed horizontal lines, where, as expected, we observe no transmission. The dark blue zone shows that no transmission takes place, while the gradual change from dark blue to red shows the increase of transmission, red being total transmission.

## 8.2 Scattering at a single relaxed micromorphic interface: Some hints towards negative-refraction-like phenomena in enriched continua

In this subsection we show the results for the reflection coefficient obtained by using the single interface boundary conditions for the relaxed micromorphic continuum as described in section 4.1.

Figure 8 shows the reflection coefficient as a function of the frequency for two different angles of incidence ( $\theta = \pi/2$  and  $\theta = \pi/4$ ), when considering an L incident wave for the “single interface” boundary conditions. Figure 9 shows the analogous results for an incident S wave. As expected, the solution obtained using the “single interface” boundary conditions, provide a sort of average behavior for the oscillation at lower frequencies. This is sensible, since when considering a semi-infinite metamaterial, multiple reflections on the two boundaries of the slab are not accounted for. The difference between “single” and “double interface” boundary conditions in the relaxed micromorphic model becomes less pronounced for higher frequencies, since the wavelength of the considered waves is expected to be much lower than the characteristic-size of the slab.

When processing the semi-analytical solution for the relaxed micromorphic model with single interface boundary conditions, we were faced with an interesting phenomenon. For frequencies higher than the band-gap and for angles of incidence smaller than normal incidence, we found a behavior provided by the relaxed micromorphic model with single interface, which could be related to what is known as negative refraction. We observed that for some frequency intervals, the third instead of the first (or the fourth instead of the second) modes had to be chosen in order to satisfy conservation of energy at the interface. This behavior has been observed for a wide range of directions of propagation and always for frequency intervals higher than the band-gap and when the two modes are simultaneously propagative (see yellow areas in Figures 10 and 11 for L and S incidence, respectively). When one of the two propagative modes is negatively refracted (in the sense we just specified), the other remains positively refracted and the sum of the two continues to be positively refracted. This phenomenon is similar to the one described in [41], where homogenization methods for a laminate composite are presented.

We acknowledge that negative refraction can also be simulated when coding a problem corresponding to the single interface, but involving all details of the microstructure. The results are only qualitative and not conclusive and further investigations are needed to obtain accurate microstructured simulation allowing the definitive validations of the relaxed micromorphic model also for higher frequencies. This delicate task is left for future work.

In any case, we point out that this negative-refraction-like phenomenon occurs in the relaxed micromorphic model without the need of having negative group velocity (the dispersion curves for the relaxed

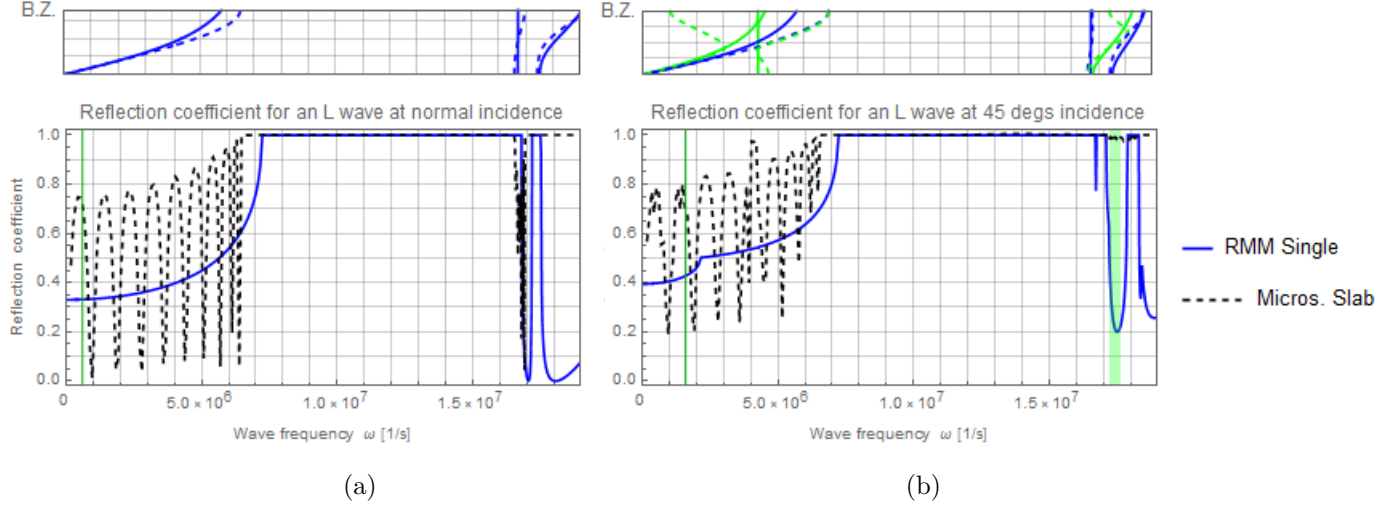


Figure 8: Reflection coefficient at the single interface for an incident L wave and for two directions of propagation  $\theta = \pi/2$  (normal incidence) (a) and  $\theta = \pi/4$  (b). The blue curve is generated by the tetragonal relaxed micromorphic model and the black dashed line indicates the microstructured model. The green vertical lines denote the long-wave limit, below which the relaxed micromorphic model is equivalent to a homogenized Cauchy model. The green shaded area is where the first transmitted mode is negatively refracted. The dispersion diagrams for  $\theta = \pi/2$  and  $\theta = \pi/4$ , given in Fig. 3 are also rotated and displayed on the top of each picture to allow for a better interpretation of results.

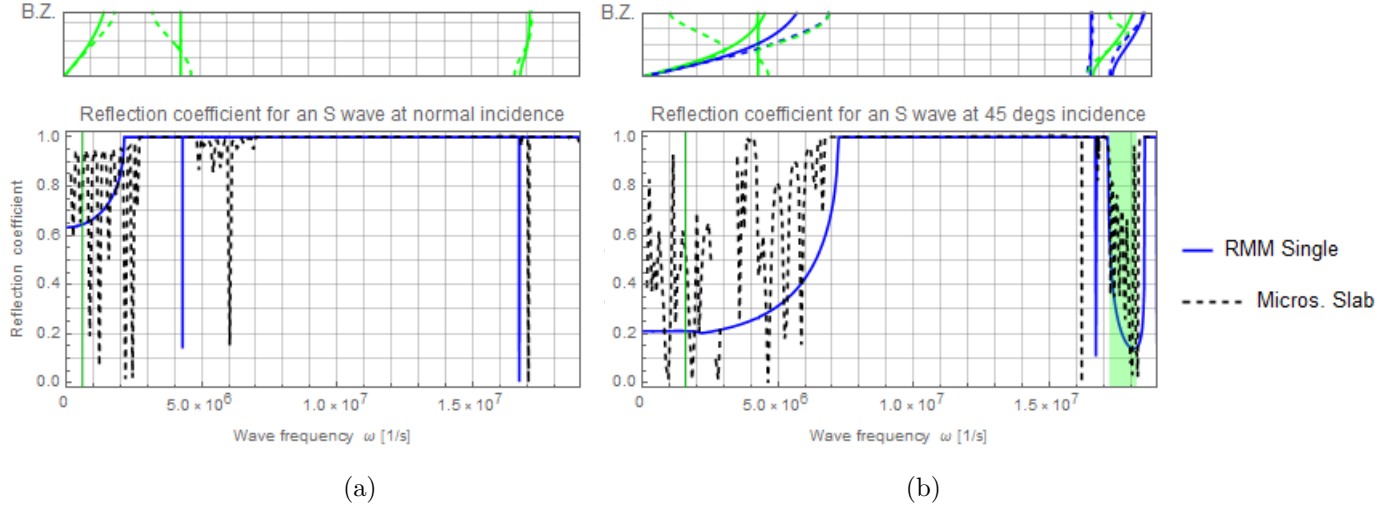


Figure 9: Reflection coefficient at the single interface for an incident S wave and for two directions of propagation  $\theta = \pi/2$  (normal incidence) (a) and  $\theta = \pi/4$  (b). The blue curve is generated by the tetragonal relaxed micromorphic model and the black dashed line indicates the microstructured model. The green vertical lines denote the long-wave limit, below which the relaxed micromorphic model is equivalent to a homogenized Cauchy model. The green shaded area is where the first transmitted mode is negatively refracted. The dispersion diagrams for  $\theta = \pi/2$  and  $\theta = \pi/4$ , given in Fig. 3 are also rotated and displayed on the top of each picture to allow for a better interpretation of results.

micromorphic model are always monotonically increasing). This may be related to the fact that group and energy velocity do not necessarily coincide when considering an anisotropic generalized continuum [34]. This specific issue requires nonetheless deeper investigation and will be addressed in further work.

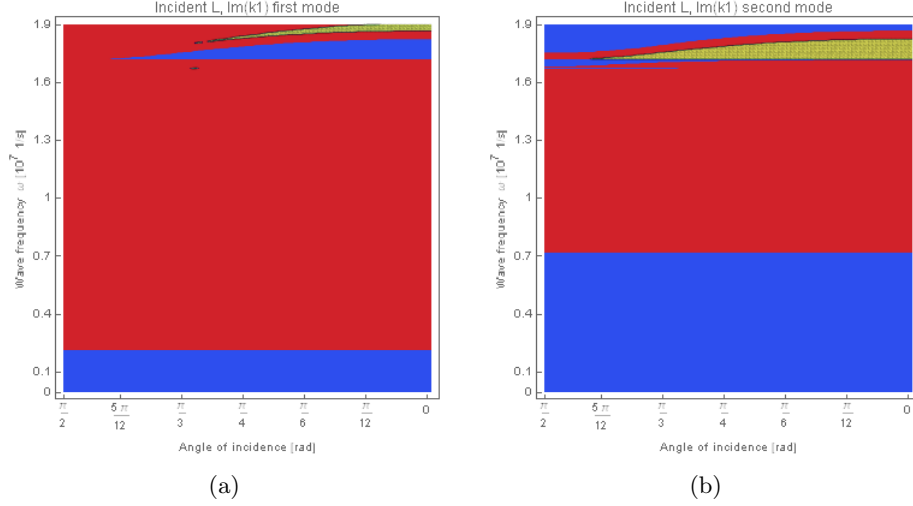


Figure 10: Values of  $\text{Im}(k_1)$  as a function of the angle of incidence  $\theta$  and of the wave-frequency  $\omega$  for the modes of the relaxed micromorphic medium and for the case of an incident L wave. The origin coincides with normal incidence ( $\theta = \pi/2$ ), while the angle of incidence decreases towards the right until it reaches the value  $\theta = 0$ , which corresponds to the limit case where the incidence is parallel to the interface. The red color in these plots means that the mode is Stoneley and does not propagate, blue means that the mode is propagative and yellow that the mode is propagative and the sign of  $k_1$  had to be switched in order to satisfy conservation of energy.

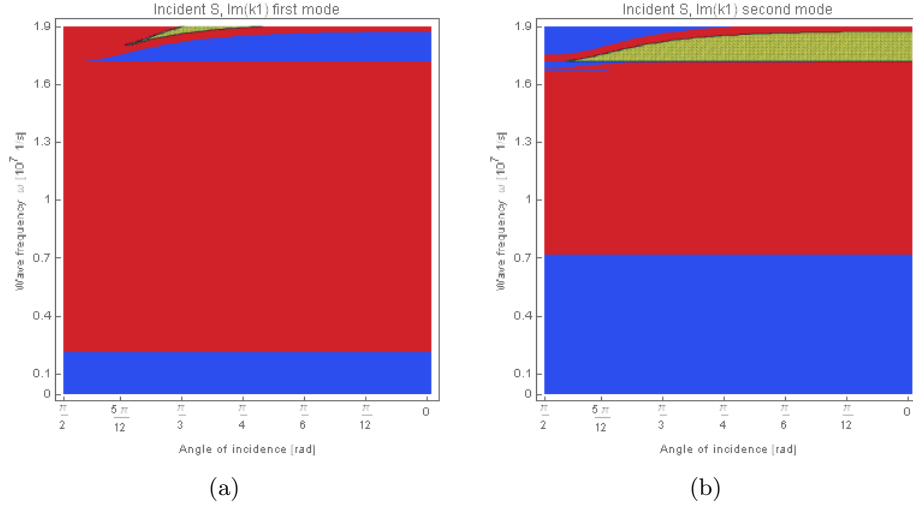


Figure 11: Values of  $\text{Im}(k_1)$  as a function of the angle of incidence  $\theta$  and of the wave-frequency  $\omega$  for the modes of the relaxed micromorphic medium and for the case of an incident L wave. The origin coincides with normal incidence ( $\theta = \pi/2$ ), while the angle of incidence decreases towards the right until it reaches the value  $\theta = 0$ , which corresponds to the limit case where the incidence is parallel to the interface. The red color in these plots means that the mode is Stoneley and does not propagate, blue means that the mode is propagative and yellow that the mode is propagative and the sign of  $k_1$  had to be switched in order to satisfy conservation of energy.

Figures 10 and 11 show the imaginary part of the modulus of the first component of the wave vectors, given in equation (3.13), as a function of the frequency and the angle of incidence for L and S incident waves, respectively. We see that, depending on the value of the frequency and of the angle of incidence, these modes can be either propagative ( $\text{Im}(k_1) \neq 0$ , blue region) or evanescent ( $\text{Im}(k_1) = 0$ , red region). In the same figures, the yellow regions indicate the frequency/angle-of-incidence regions for which the sign of the mode must be changed (negative instead of positive) in order to verify conservation of energy at the interface. This negative refraction-like phenomenon is observed here for the first time in the relaxed micromorphic model and is interesting in itself. More accurate investigation is nonetheless needed to better understand its possibilities of application.

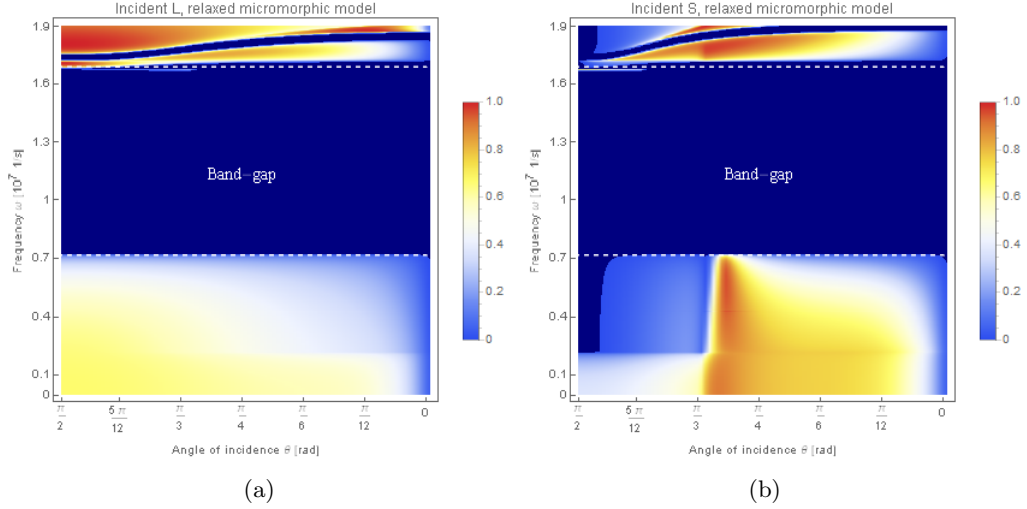


Figure 12: Transmission coefficient of the single interface as a function of the angle of incidence  $\theta$  and of the wave-frequency  $\omega$ . Panel (a) depicts the case of an incident L wave, while panel (b) the case of an incident S wave. The origin coincides with normal incidence ( $\theta = \pi/2$ ), while the angle of incidence decreases towards the right until it reaches the value  $\theta = 0$ , which corresponds to the limit case where the incidence is parallel to the interface. The band-gap region is highlighted by two dashed horizontal lines, where, as expected, we observe no transmission. The dark blue zone shows that no transmission takes place, while the gradual change from dark blue to red shows the increase of transmission, red being total transmission.

We conclude this subsection by showing the transmission coefficients at the “single interface”, as a function of the frequency and the angle of incidence for L and S incident waves (Fig. 12(a) and 12(b), respectively). Comparing Fig. 6(b) to 12(a) and 7(b) to 12(b), we can visualize the extent to which the single interface can be considered to represent a metastructure of finite size. Although some basic averaged information is contained in Figures 12(a) and 12(b) (band-gap, critical angles), the detailed scattering behavior of the finite slab cannot be inferred from it. This provides additional evidence for the real need to propose a framework in which macroscopic boundary conditions can be introduced in a simplified way. Semi-infinite problems for metamaterials are solved in the context of homogenization methods in [36, 38], but to the author’s knowledge, the rigorous solution of scattering problems for metamaterials of finite size is not available in the literature.

## 9 Conclusions

In this paper we presented for the first time the scattering solution of a metamaterial slab of finite size, modeled via a rigorous boundary value problem describing its homogenized behavior.

The correct macroscopic boundary conditions (continuity of macroscopic displacement and of generalized tractions) are presented and are intrinsically compatible with the used macroscopic bulk PDEs. The scattering properties of the considered finite-size metastructures, as obtained via the relaxed micromorphic model, are compared to a direct microstructured simulation. This simulation is obtained by assuming that the metamaterial’s unit cell is periodic and linear-elastic. Excellent agreement is found for all angles of incidence and for frequencies going from the long-wave limit to the first band-gap and beyond. Further work will be devoted to better understanding the high-frequency behavior of the considered metamaterials so as to provide a final validation of the relaxed micromorphic model also for such higher frequencies.

The results presented in this paper open the way to the future study of the scattering properties of more complex 2D or 3D finite-sized metastructures in a simplified macroscopic environment.

## Acknowledgements

Angela Madeo and Domenico Tallarico acknowledge funding from the French Research Agency ANR, “METASMART” (ANR-17CE08-0006). Angela Madeo acknowledges support from IDEXLYON in the framework of the “Programme Investissement d’Avenir” ANR-16-IDEX-0005. All the authors acknowledge funding from the “Région Auvergne-Rhône-Alpes” for the “SCUSI” project for international mobility France/Germany.

## A Appendix

### A.1 Energy flux for the anisotropic relaxed micromorphic model

#### A.1.1 Derivation of expression (2.10)

The total energy is given by:

$$E = J(u, t, \nabla u, t, P, t) + W(\nabla u, P, \text{Curl } P), \quad (\text{A.1})$$

where  $J(u, t, \nabla u, t, P, t)$  and  $W(\nabla u, P, \text{Curl } P)$  are defined in (2.5) and (2.6). Differentiating (A.1) with respect to time<sup>13</sup> we have:

$$\begin{aligned} E_{,t} = & \langle u, t, \rho u, tt \rangle + \langle \text{sym } P, t, \mathbb{J}_{\text{micro}} \text{sym } P, tt \rangle + \langle \text{skew } P, t, \mathbb{J}_c \text{skew } P, tt \rangle + \langle \text{sym } \nabla u, t, \mathbb{T}_e \text{sym } \nabla u, tt \rangle \\ & + \langle \text{skew } \nabla u, t, \mathbb{T}_c \text{skew } \nabla u, tt \rangle + \langle \mathbb{C}_e \text{sym}(\nabla u - P), \text{sym}(\nabla u - P), t \rangle + \langle \mathbb{C}_c \text{skew}(\nabla u - P), \text{skew}(\nabla u - P), t \rangle \\ & + \langle \mathbb{C}_{\text{micro}} \text{sym } P, \text{sym } P, t \rangle + L_c^2 (\langle \mathbb{L}_e \text{sym } \text{Curl } P, \text{sym } \text{Curl } P, t \rangle + \langle \mathbb{L}_c \text{skew } \text{Curl } P, \text{skew } \text{Curl } P, t \rangle). \end{aligned} \quad (\text{A.5})$$

Using the governing equations (2.8), definitions (2.9) for  $\tilde{\sigma}, \hat{\sigma}, s, m$  and (A.2), (A.3), (A.4) we have:

$$\begin{aligned} \langle u, t, \rho u, tt \rangle &= \langle u, t, \text{Div}(\mathbb{T}_e \text{sym } \nabla u, tt + \mathbb{T}_c \text{skew } \nabla u, tt) + \text{Div } \tilde{\sigma} \rangle \\ &= \langle u, t, \text{Div } \tilde{\sigma} \rangle + \langle u, t, \text{Div}(\underbrace{\mathbb{T}_e \text{sym } \nabla u, tt + \mathbb{T}_c \text{skew } \nabla u, tt}_{:=\hat{\sigma}}) \rangle \\ &= \langle u, t, \text{Div } \tilde{\sigma} \rangle + \langle u, t, \text{Div } \hat{\sigma} \rangle, \\ \langle \text{sym } P, t, \mathbb{J}_{\text{micro}} \text{sym } P, tt \rangle + \langle \text{skew } P, t, \mathbb{J}_c \text{skew } P, tt \rangle &= \langle \text{sym } P, t + \text{skew } P, t, \mathbb{J}_{\text{micro}} \text{sym } P, tt \rangle + \langle \text{sym } P, t + \text{skew } P, t, \mathbb{J}_c \text{skew } P, tt \rangle \\ &= \langle P, t, \mathbb{J}_{\text{micro}} \text{sym } P, tt + \mathbb{J}_c \text{skew } P, tt \rangle = \langle P, t, \tilde{\sigma}_e - s - \text{sym } \text{Curl } m + \tilde{\sigma}_c - \text{skew } \text{Curl } m \rangle \\ &= \langle P, t, \tilde{\sigma} - s - \text{Curl } m \rangle = \langle P, t, \tilde{\sigma} \rangle - \langle P, t, s \rangle - \langle P, t, \text{Curl } m \rangle, \\ \langle \text{sym } \nabla u, t, \mathbb{T}_e \text{sym } \nabla u, tt \rangle + \langle \text{skew } \nabla u, t, \mathbb{T}_c \text{skew } \nabla u, tt \rangle &= \langle \text{sym } \nabla u, t + \text{skew } \nabla u, t, \mathbb{T}_e \text{sym } \nabla u, tt \rangle + \langle \text{sym } \nabla u, t + \text{skew } \nabla u, t, \mathbb{T}_c \text{skew } \nabla u, tt \rangle \\ &= \langle \nabla u, t, \underbrace{\mathbb{T}_e \text{sym } \nabla u, tt + \mathbb{T}_c \text{skew } \nabla u, tt}_{:=\hat{\sigma}} \rangle = \langle \nabla u, t, \hat{\sigma} \rangle = \text{Div}(u, t \cdot \hat{\sigma}) - \langle u, t, \text{Div } \hat{\sigma} \rangle, \\ \langle \mathbb{C}_e \text{sym}(\nabla u - P), \text{sym}(\nabla u - P), t \rangle + \langle \mathbb{C}_c \text{skew}(\nabla u - P), \text{skew}(\nabla u - P), t \rangle &= \langle \mathbb{C}_e \text{sym}(\nabla u - P), \text{sym}(\nabla u - P), t \rangle + \langle \text{skew}(\nabla u - P), t \rangle \\ &+ \langle \mathbb{C}_c \text{skew}(\nabla u - P), \text{sym}(\nabla u - P), t \rangle + \langle \text{skew}(\nabla u - P), t \rangle \\ &= \langle \mathbb{C}_e \text{sym}(\nabla u - P) + \mathbb{C}_c \text{skew}(\nabla u - P), (\nabla u - P), t \rangle = \langle \tilde{\sigma}, (\nabla u - P), t \rangle \\ &= \langle \tilde{\sigma}, \nabla u, t \rangle - \langle \tilde{\sigma}, P, t \rangle = \text{Div}(u, t \cdot \tilde{\sigma}) - \langle u, t, \text{Div } \tilde{\sigma} \rangle - \langle \tilde{\sigma}, P, t \rangle, \\ \langle \mathbb{C}_{\text{micro}} \text{sym } P, \text{sym } P, t \rangle = \langle \mathbb{C}_{\text{micro}} \text{sym } P, \text{sym } P, t + \text{skew } P, t \rangle = \langle \mathbb{C}_{\text{micro}} \text{sym } P, P, t \rangle = \langle s, P, t \rangle, \\ L_c^2 (\langle \mathbb{L}_e \text{sym } \text{Curl } P, \text{sym } \text{Curl } P, t \rangle + \langle \mathbb{L}_c \text{skew } \text{Curl } P, \text{skew } \text{Curl } P, t \rangle) &= L_c^2 (\langle \mathbb{L}_e \text{sym } \text{Curl } P, \text{sym } \text{Curl } P, t + \text{skew } \text{Curl } P, t \rangle + \langle \mathbb{L}_c \text{skew } \text{Curl } P, \text{sym } \text{Curl } P, t + \text{skew } \text{Curl } P, t \rangle) \\ &= \langle L_c^2 (\mathbb{L}_e \text{sym } \text{Curl } P + \mathbb{L}_c \text{skew } \text{Curl } P), \text{Curl } P, t \rangle = \langle m, \text{Curl } P, t \rangle = \text{Div} \left( (m^T \cdot P, t) : \epsilon \right) - \langle \text{Curl } m, P, t \rangle. \end{aligned}$$

So, by adding all the above and simplifying (A.5) becomes:

$$E_{,t} = \text{Div} \left[ (\tilde{\sigma} + \hat{\sigma})^T \cdot u, t + (m^T \cdot P, t) : \epsilon \right], \quad (\text{A.6})$$

from which we can define the energy flux for the general anisotropic relaxed micromorphic model:

$$H = -(\tilde{\sigma} + \hat{\sigma})^T \cdot u, t - (m^T \cdot P, t) : \epsilon. \quad (\text{A.7})$$

---

<sup>13</sup>Let  $\psi$  be a vector field and  $A$  a second order tensor field. Then

$$\langle \nabla \psi, A \rangle = \text{Div}(\psi \cdot A) - \langle \psi, \text{Div } A \rangle. \quad (\text{A.2})$$

Taking  $\psi = u, t$  and  $A = \tilde{\sigma}$  we have

$$\langle \nabla u, t, \tilde{\sigma} \rangle = \text{Div}(u, t \cdot \tilde{\sigma}) - \langle u, t, \text{Div } \tilde{\sigma} \rangle. \quad (\text{A.3})$$

Furthermore, we have the following identity

$$\langle m, \text{Curl } P, t \rangle = \text{Div} \left( (m^T \cdot P, t) : \epsilon \right) + \langle \text{Curl } m, P, t \rangle, \quad (\text{A.4})$$

which follows from the identity  $\text{div}(v \times w) = w \cdot \text{curl } v - v \cdot \text{curl } w$ , where  $v, w$  are suitable vector fields,  $\times$  is the usual vector product and  $:$  is the double contraction between tensors.

### A.1.2 Analytical expression of the flux for the relaxed micromorphic model when $L_c = 0$

The flux  $H$  of the relaxed micromorphic model when  $L_c = 0$  can be written as (using Lemma 1)

$$H = \frac{1}{2} \text{Re} \left[ (\alpha_1 \omega (-2\omega^2 \mathcal{A} + \mathcal{B}) + \alpha_2 \omega (-2\omega^2 \mathcal{C} + \mathcal{D})) \mathcal{E}^* + (\alpha_1 \omega (\mathcal{F} + \omega \mathcal{G} + \omega^2 \mathcal{H}) + \alpha_2 \omega (\mathcal{I} + \omega \mathcal{J} + \omega^2 \mathcal{K})) \mathcal{L}^* \right], \quad (\text{A.8})$$

with

$$\begin{aligned} \mathcal{A} &= k_1^{(1)} \phi_1^{(1)} \left( \bar{\eta}_1 + \frac{1}{2} \bar{\eta}_3 \right) + k_0 \phi_2^{(1)} \bar{\eta}_3, \\ \mathcal{B} &= (\lambda_e + 2\mu_e) \left( k_1^{(1)} \phi_1^{(1)} - \phi_3^{(1)} \omega \right) + \lambda_e \left( k_0 \phi_2^{(1)} - \phi_6^{(1)} \omega \right), \\ \mathcal{C} &= k_1^{(2)} \phi_1^{(2)} \left( \bar{\eta}_1 + \frac{1}{2} \bar{\eta}_3 \right) + k_0 \phi_2^{(2)} \bar{\eta}_3, \\ \mathcal{D} &= (\lambda_e + 2\mu_e) \left( k_1^{(2)} \phi_1^{(2)} - \phi_3^{(2)} \omega \right) + \lambda_e \left( k_0 \phi_2^{(2)} - \phi_6^{(2)} \omega \right), \\ \mathcal{E} &= \alpha_1 \phi_1^{(1)} + \alpha_2 \phi_1^{(2)}, \\ \mathcal{F} &= k_0 (\mu_e^* - \mu_c) \phi_1^{(1)} + k_1^{(1)} (\mu_e^* + \mu_c) \phi_2^{(1)}, \\ \mathcal{G} &= -(\mu_e^* - \mu_c) \phi_4^{(1)} - (\mu_e^* + \mu_c) \phi_5^{(1)}, \\ \mathcal{H} &= k_0 \phi_1^{(1)} \left( \frac{1}{4} \bar{\eta}_2 - \bar{\eta}^* \right) - k_1^{(1)} \phi_2^{(1)} \left( \frac{1}{4} \bar{\eta}_2 + \bar{\eta}^* \right), \\ \mathcal{I} &= k_0 (\mu_e^* - \mu_c) \phi_1^{(2)} + k_1^{(2)} (\mu_e^* + \mu_c) \phi_2^{(2)}, \\ \mathcal{J} &= -(\mu_e^* - \mu_c) \phi_4^{(2)} - (\mu_e^* + \mu_c) \phi_5^{(2)}, \\ \mathcal{K} &= k_0 \phi_1^{(2)} \left( \frac{1}{4} \bar{\eta}_2 - \bar{\eta}^* \right) - k_1^{(2)} \phi_2^{(1)} \left( \frac{1}{4} \bar{\eta}_2 + \bar{\eta}^* \right), \\ \mathcal{L} &= \alpha_1 \phi_2^{(1)} + \alpha_2 \phi_2^{(2)}. \end{aligned} \quad (\text{A.9})$$

## A.2 The matrix $\hat{A}$

We present the matrix row-wise. We have

$$\begin{aligned} \hat{A}_1 &= \begin{pmatrix} -(\rho + k_1^2(2\bar{\eta}_1 + \bar{\eta}_3) + k_2^2(\frac{1}{4}\bar{\eta}_2 + \bar{\eta}_1^*)) \omega^2 + k_1^2(\lambda_e + 2\mu_e) + k_2^2(\mu_c + \mu_e^*) \\ k_1 k_2 (\frac{1}{4}\bar{\eta}_2 - \bar{\eta}_3 + \bar{\eta}_1^*) \omega^2 + k_1 k_2 (\lambda_e - \mu_c + \mu_e^*) \\ i k_1 (\lambda_e + 2\mu_e) \\ i k_2 (\mu_c + \mu_e^*) \\ i k_2 (-\mu_c + \mu_e^*) \\ i k_1 \lambda_e \end{pmatrix}^T, \\ \hat{A}_2 &= \begin{pmatrix} k_1 k_2 (\frac{1}{4}\bar{\eta}_2 - \bar{\eta}_3 - \bar{\eta}_1^*) \omega^2 + k_1 k_2 (\lambda_e - \mu_c + \mu_e^*) \\ -(\rho + k_2^2(2\bar{\eta}_1 + \bar{\eta}_3) + k_1^2(\frac{1}{4}\bar{\eta}_2 + \bar{\eta}_1^*)) \omega^2 + k_2^2(\lambda_e + 2\mu_e) + k_1^2(\mu_c + \mu_e^*) \\ i k_2 \lambda_e \\ -i k_1 (\mu_c - \mu_e^*) \\ i k_1 (\mu_e + \mu_e^*) \\ i k_2 (\lambda_e + 2\mu_e) \end{pmatrix}^T, \\ \hat{A}_3 &= \begin{pmatrix} -i k_1 (\lambda_e + 2\mu_e) \\ -i k_2 \lambda_e \\ -(2\eta_1 + \eta_3) \omega^2 + \lambda_e + \lambda_{\text{micro}} + 2(\mu_e + \mu_{\text{micro}}) + k_2^2 L_c^2 \\ -k_1 k_2 L_c^2 \\ 0 \\ -\eta_3 \omega^2 + \lambda_e + \lambda_{\text{micro}} \end{pmatrix}^T, \quad \hat{A}_4 = \begin{pmatrix} -i k_2 (\mu_c + \mu_e^*) \\ i k_1 (\mu_c - \mu_e^*) \\ -k_1 k_2 L_c^2 \\ -(\eta_2 + \eta_1^*) \omega^2 + \mu_c + \mu_e^* + \mu_{\text{micro}}^* + k_1^2 L_c^2 \\ (\eta_2 - \eta_1^*) \omega^2 - \mu_c + \mu_e^* + \mu_{\text{micro}}^* \\ 0 \end{pmatrix}^T, \end{aligned}$$

$$\hat{A}_5 = \begin{pmatrix} i k_2(\mu_c - \mu_e^*) \\ -i k_1(\mu_c + \mu_e^*) \\ 0 \\ (\eta_2 - \eta_1^*)\omega^2 - \mu_c + \mu_e^* + \mu_{\text{micro}}^* \\ -(\eta_2 + \eta_1^*)\omega^2 + \mu_c + \mu_e^* + \mu_{\text{micro}}^* + k_2^2 L_c^2 \\ -k_1 k_2 L_c^2 \end{pmatrix}^T, \quad \hat{A}_6 = \begin{pmatrix} -i k_1 \lambda_e \\ -i k_2(\lambda_e + 2\mu_e) \\ -\eta_3 \omega^2 + \lambda_e + \lambda_{\text{micro}} \\ 0 \\ -k_1 k_2 L_c^2 \\ -(2\eta_1 + \eta_3)\omega^2 + \lambda_e + \lambda_{\text{micro}} + 2(\mu_e + \mu_{\text{micro}}) + k_1^2 L_c^2 \end{pmatrix}^T,$$

Then, the matrix  $\hat{A}$  is

$$\hat{A} = (\hat{A}_1, \hat{A}_2, \hat{A}_3, \hat{A}_4, \hat{A}_5, \hat{A}_6)^T \quad (\text{A.10})$$

### A.3 Lemma 1

We have the following well-known result.

*Lemma 1.* Let

$$u_1(x, t) = A(x)e^{i(\omega t - kx)}, \quad u_2(x, t) = B(x)e^{i(\omega t - kx)}$$

be two functions with  $A, B : \mathbb{R}^3 \rightarrow \mathbb{C}$ . Then the following holds

$$\frac{1}{T} \int_0^T \text{Re}\{u_1(x, t)\} \text{Re}\{u_2(x, t)\} dt = \frac{1}{2} \text{Re}(AB^*), \quad (\text{A.11})$$

where  $T$  is the period of the functions  $u_1, u_2$  and  $B^*$  denotes the complex conjugate.

*Proof.* We have:

$$\begin{aligned} \frac{1}{T} \int_0^T \text{Re}\{u_1(x, t)\} \text{Re}\{u_2(x, t)\} dt &= \frac{1}{T} \int_0^T \text{Re}\left(Ae^{i(\omega t - kx)}\right) \text{Re}\left(Be^{i(\omega t - kx)}\right) dt \\ &= \frac{1}{T} \int_0^T \frac{Ae^{i(\omega t - kx)} + A^*e^{-i(\omega t - kx)}}{2} \frac{Be^{i(\omega t - kx)} + B^*e^{-i(\omega t - kx)}}{2} dt \\ &= \frac{1}{T} \int_0^T \frac{AB}{4} \underbrace{e^{2i\omega t}}_{\text{periodic}} e^{2ikx} + \frac{AB^*}{4} + \frac{A^*B}{4} + \frac{A^*B^*}{4} \underbrace{e^{2i\omega t}}_{\text{periodic}} e^{2ikx} dt \\ &= \frac{1}{T} \int_0^T \frac{AB^* + A^*B}{4} dt = \frac{1}{2T} \int_0^T \text{Re}(AB^*) dt = \frac{1}{2} \text{Re}(AB^*), \end{aligned} \quad (\text{A.12})$$

where we used the facts that the periodic function  $e^{2i\omega t}$  integrated over its period is zero and that for any complex number  $z \in \mathbb{C}$ :  $\text{Re}(z) = \frac{z+z^*}{2}$ . ■

## References

- [1] Alexios Aivaliotis, Ali Daouadji, Gabriele barbagall, Domenico Tallarico, Patrizio Neff, and Angela Madeo. Microstructure-related stoneley waves and their effect on the scattering properties of a 2d cauchy/relaxed micromorphic interface. *to appear on Wave Motion*, 2019.
- [2] Alexios Aivaliotis, Ali Daouadji, Gabriele Barbagallo, Domenico Tallarico, Patrizio Neff, and Angela Madeo. Low-and high-frequency stoneley waves, reflection and transmission at a cauchy/relaxed micromorphic interface. *arXiv preprint arXiv:1810.12578*, 2018.
- [3] Bertram A. Auld. *Acoustic Fields and Waves in Solids, Vol. I*. Wiley-Interscience Publication, 1973.
- [4] Gabriele Barbagallo, Angela Madeo, Marco Valerio d’Agostino, Rafael Abreu, Ionel-Dumitrel Ghiba, and Patrizio Neff. Transparent anisotropy for the relaxed micromorphic model: macroscopic consistency conditions and long wave length asymptotics. *International Journal of Solids and Structures*, 120:7–30, 2017.
- [5] Gabriele Barbagallo, Domenico Tallarico, Marco Valerio d’Agostino, Alexios Aivaliotis, Patrizio Neff, and Angela Madeo. Relaxed micromorphic model of transient wave propagation in anisotropic band-gap metastructures. *International Journal of Solids and Structures*, 2018.
- [6] Ushnish Basu and Anil K. Chopra. Perfectly matched layers for time-harmonic elastodynamics of unbounded domains: theory and finite-element implementation. *Computer methods in applied mechanics and engineering*, 192(11-12):1337–1375, 2003.

- [7] Felix Bloch. Über die Quantenmechanik der Elektronen in Kristallgittern. *Zeitschrift für Physik*, 52(7-8):555–600, 1929.
- [8] Huanyang Chen and Che Ting Chan. Acoustic cloaking and transformation acoustics. *Journal of Physics D: Applied Physics*, 43(11):113001, 2010.
- [9] Richard V. Craster and Sébastien Guenneau. *Acoustic metamaterials: Negative refraction, imaging, lensing and cloaking*, volume 166. Springer Science & Business Media, 2012.
- [10] Marco Valerio d’Agostino, Gabriele Barbagallo, Ionel-Dumitrel Ghiba, Bernhard Eidel, Patrizio Neff, and Angela Madeo. Effective description of anisotropic wave dispersion in mechanical band-gap metamaterials via the relaxed micromorphic model. *submitted, arXiv preprint*, 1709.07054, 2018.
- [11] Ahmed Cemal Eringen. *Microcontinuum field theories*. Springer-Verlag, New York, 1999.
- [12] Gaston Floquet. Sur les equations differentielles lineaires. *Ann. ENS [2]*, 12(1883):47–88, 1883.
- [13] Marc G.D. Geers, Varvara G. Kouznetsova, and W.A.M. Brekelmans. Multi-scale computational homogenization: Trends and challenges. *Journal of computational and applied mathematics*, 234(7):2175–2182, 2010.
- [14] Muamer Kadic, Tiemo Bückmann, Robert Schittny, and Martin Wegener. Metamaterials beyond electromagnetism. *Reports on Progress in Physics*, 76(12):126501, 2013.
- [15] Anastasiia O. Krushynska, Varvara G. Kouznetsova, and Marc G.D. Geers. Towards optimal design of locally resonant acoustic metamaterials. *Journal of the Mechanics and Physics of Solids*, 71:179–196, 2014.
- [16] John Leckner. *Theory of Reflection: Reflection and Transmission of Electromagnetic, Particle and Acoustic Waves*. New York., John Wiley & Sons, 1973.
- [17] Angela Madeo, Gabriele Barbagallo, Manuel Collet, Marco Valerio d’Agostino, Marco Miniaci, and Patrizio Neff. Relaxed micromorphic modeling of the interface between a homogeneous solid and a band-gap metamaterial: New perspectives towards metastructural design. *Mathematics and Mechanics of Solids*, pages 1–22, 2017.
- [18] Angela Madeo, Gabriele Barbagallo, Marco Valerio d’Agostino, Luca Placidi, and Patrizio Neff. First evidence of non-locality in real band-gap metamaterials: determining parameters in the relaxed micromorphic model. *Proceedings of the Royal Society A: Mathematical, Physical and Engineering Sciences*, 472(2190):20160169, 2016.
- [19] Angela Madeo, Manuel Collet, Marco Miniaci, Kévin Billon, Morvan Ouisse, and Patrizio Neff. Modeling phononic crystals via the weighted relaxed micromorphic model with free and gradient micro-inertia. *Journal of Elasticity*, 130(1):59–83, 2017.
- [20] Angela Madeo, Patrizio Neff, Elias C. Aifantis, Gabriele Barbagallo, and Marco Valerio d’Agostino. On the role of micro-inertia in enriched continuum mechanics. *Proceedings of the Royal Society A: Mathematical, Physical and Engineering Science*, 473(2198):20160722, 2017.
- [21] Angela Madeo, Patrizio Neff, Gabriele Barbagallo, Marco Valerio d’Agostino, and Ionel-Dumitrel Ghiba. A review on wave propagation modeling in band-gap metamaterials via enriched continuum models. In Francesco dell’Isola, Mircea Sofonea, and David J. Steigmann, editors, *Mathematical Modelling in Solid Mechanics*, Advanced Structured Materials, pages 89–105. Springer, Singapore, 2017.
- [22] Angela Madeo, Patrizio Neff, Marco Valerio d’Agostino, and Gabriele Barbagallo. Complete band gaps including non-local effects occur only in the relaxed micromorphic model. *Comptes Rendus Mécanique*, 344(11-12):784–796, 2016.
- [23] Angela Madeo, Patrizio Neff, Ionel-Dumitrel Ghiba, Luca Placidi, and Giuseppe Rosi. Band gaps in the relaxed linear micromorphic continuum. *Zeitschrift für Angewandte Mathematik und Mechanik*, 95(9):880–887, 2014.
- [24] Angela Madeo, Patrizio Neff, Ionel-Dumitrel Ghiba, Luca Placidi, and Giuseppe Rosi. Wave propagation in relaxed micromorphic continua: modeling metamaterials with frequency band-gaps. *Continuum Mechanics and Thermodynamics*, 27(4-5):551–570, 2015.
- [25] Angela Madeo, Patrizio Neff, Ionel-Dumitrel Ghiba, and Giuseppe Rosi. Reflection and transmission of elastic waves in non-local band-gap metamaterials: a comprehensive study via the relaxed micromorphic model. *Journal of the Mechanics and Physics of Solids*, 95:441–479, 2016.
- [26] Raymond David Mindlin. Micro-structure in linear elasticity. *Archive for Rational Mechanics and Analysis*, 16(1):51–78, 1964.
- [27] Diego Misseroni, Daniel J. Colquitt, Alexander B. Movchan, Natasha V. Movchan, and Ian Samuel Jones. Cymatics for the cloaking of flexural vibrations in a structured plate. *Scientific Reports*, 6(23929), 2016.
- [28] Patrizio Neff, Ionel-Dumitrel Ghiba, Markus Lazar, and Angela Madeo. The relaxed linear micromorphic continuum: well-posedness of the static problem and relations to the gauge theory of dislocations. *The Quarterly Journal of Mechanics and Applied Mathematics*, 68(1):53–84, 2015.
- [29] Patrizio Neff, Ionel-Dumitrel Ghiba, Angela Madeo, Luca Placidi, and Giuseppe Rosi. A unifying perspective: the relaxed linear micromorphic continuum. *Continuum Mechanics and Thermodynamics*, 26(5):639–681, 2014.

- [30] Patrizio Neff, Angela Madeo, Gabriele Barbagallo, Marco Valerio d’Agostino, Rafael Abreu, and Ionel-Dumitrel Ghiba. Real wave propagation in the isotropic-relaxed micromorphic model. *Proceedings of the Royal Society A: Mathematical, Physical and Engineering Sciences*, 473(2197):20160790, 2017.
- [31] Andrew N. Norris. Acoustic cloaking. *Acoustics Today*, 11(1):38, 46.
- [32] Sebastian Owczarek, Ionel-Dumitrel Ghiba, Marco-Valerio d’Agostino, and Patrizio Neff. Nonstandard micro-inertia terms in the relaxed micromorphic model: well-posedness for dynamics. *to appear in Mathematics and Mechanics of Solids*, 2018.
- [33] Steven B. Platts, Natalia V. Movchan, Ross C. McPhedran, and Alexander B. Movchan. Two-dimensional phononic crystals and scattering of elastic waves by an array of voids. 458(2026):2327–2347, 2002.
- [34] Giuseppe Rosi and Nicolas Auffray. Anisotropic and dispersive wave propagation within strain-gradient framework. *Wave Motion*, 63:120–134, 2016.
- [35] Ashwin Sridhar, Varvara G. Kouznetsova, and Marc G.D. Geers. A general multiscale framework for the emergent effective elastodynamics of metamaterials. *Journal of the Mechanics and Physics of Solids*, 111:414–433, 2018.
- [36] Ankit Srivastava and John R. Willis. Evanescent wave boundary layers in metamaterials and sidestepping them through a variational approach. *Proc. R. Soc. A*, 473(2200):20160765, 2017.
- [37] John R. Willis. Dynamics of composites. In *Continuum micromechanics*, pages 265–290. Springer, 1997.
- [38] John R. Willis. Exact effective relations for dynamics of a laminated body. *Mechanics of Materials*, 41(4):385–393, 2009.
- [39] John R. Willis. Effective constitutive relations for waves in composites and metamaterials. In *Proceedings of the Royal Society of London A: Mathematical, Physical and Engineering Sciences*, volume 467, pages 1865–1879. The Royal Society, 2011.
- [40] John R. Willis. The construction of effective relations for waves in a composite. *Comptes Rendus Mécanique*, 340(4-5):181–192, 2012.
- [41] John R. Willis. Negative refraction in a laminate. *Journal of the Mechanics and Physics of Solids*, 97:10–18, 2016.